

1 **Oligomer formation from the gas-phase reactions of Criegee**
2 **intermediates with hydroperoxide esters: mechanism and kinetics**

3 Long Chen,^{1,2} Yu Huang,^{*,1,2} Yonggang Xue,^{1,2} Zhihui Jia,³ Wenliang Wang⁴

4 ¹ *State Key Lab of Loess and Quaternary Geology (SKLLQG), Institute of Earth*
5 *Environment, Chinese Academy of Sciences (CAS), Xi'an, 710061, China*

6 ² *CAS Center for Excellence in Quaternary Science and Global Change, Xi'an, 710061,*
7 *China*

8 ³ *School of Materials Science and Engineering, Shaanxi Normal University, Xi'an,*
9 *Shaanxi, 710119, China*

10 ⁴ *School of Chemistry and Chemical Engineering, Key Laboratory for Macromolecular*
11 *Science of Shaanxi Province, Shaanxi Normal University, Xi'an, Shaanxi, 710119,*
12 *China*

13

14

15

16 Submitted to *Atmospheric Chemistry & Physics*

17

18

19 *Corresponding author:

20 Prof. Yu Huang, E-mail address: huangyu@ieecas.cn

21

22 **Abstract**

23 Hydroperoxide esters, formed in the reactions of carbonyl oxides (also called
24 Criegee intermediates, CIs) with formic acid, play a crucial role in the formation of
25 secondary organic aerosol (SOA) in the atmosphere. However, the transformation
26 mechanism of hydroperoxide esters in the presence of stabilized Criegee intermediates
27 (SCIs) is not well understood. Herein, the oligomerization reaction mechanisms and
28 kinetics of distinct SCIs (CH_2OO , *syn*- CH_3CHOO , *anti*- CH_3CHOO and $(\text{CH}_3)_2\text{COO}$)
29 reactions with their respective hydroperoxide esters as well as with hydroperoxymethyl
30 formate (HPMF) are investigated in the gas phase using quantum chemical and kinetics
31 modeling methods. The calculations show that the addition reactions of SCIs with
32 hydroperoxide esters proceed through successive insertion of SCIs into hydroperoxide
33 ester to form oligomers that involve SCIs as the repeated chain unit. The exothermicity
34 of oligomerization reactions significantly decreases when the number of methyl
35 substituents increases, and the exothermicity of *anti*-methyl substituted carbonyl oxides
36 is obviously higher than that of *syn*-methyl substituted carbonyl oxides. The $-\text{OOH}$
37 insertion reaction is energetically more feasible than the $-\text{CH}$ insertion pathway in the
38 SCIs oligomerization reactions, and the barrier heights increase with increasing the
39 number of SCIs added to the oligomer except *syn*- CH_3CHOO . For the reactions of
40 distinct SCIs with HPMF, the barrier of $-\text{OOH}$ insertion pathway shows a dramatic
41 decrease when a methyl substituent occurs at the *anti*-position, while it reveals a
42 significant increase when a methyl group is introduced at the *syn*-position and dimethyl
43 substituent. Compared with the rate coefficients of the $\text{CH}_2\text{OO} + \text{HPMF}$ reaction, the
44 rate coefficients increase by about one order of magnitude when a methyl substituent
45 occurs at the *anti*-position, whereas the rate coefficients decrease by 1-2 orders of
46 magnitude when a methyl group is introduced at the *syn*-position. These new findings
47 advance our current understanding on the influence of Criegee-chemistry on the
48 formation processes and chemical compositions of SOA.

49

50 **1. Introduction**

51 Alkenes are an important class of volatile organic compounds (VOCs) that are
52 emitted into the atmosphere from large quantities of biogenic and anthropogenic
53 sources (Lester and Klippenstein, 2018). The reaction with ozone is one of the dominant
54 degradation pathways for alkenes in the atmosphere (Johnson and Marston, 2008;
55 Atkinson and Arey, 2003). Ozonolysis of alkene proceeds through the electrophilic 1,3-
56 cycloaddition of ozone to C=C bond of alkenes to form a primary ozonides (POZ), and
57 then it rapidly decomposes into a carbonyl compound and a carbonyl oxide (also called
58 Criegee intermediates, CIs) (Criegee, 1975; Osborn and Taatjes, 2015; Giorio et al.,
59 2017). A part of the initially energized CIs (~ 37-50%) may promptly dissociate to OH
60 radicals, which are thought to be an important nonphotolytic source of OH radicals in
61 the atmosphere (Novelli et al., 2014; Liu et al., 2014). The remaining CIs (~ 63-50%)
62 are collisionally stabilized prior to the thermal unimolecular decay (Lester and
63 Klippenstein, 2018; Novelli et al., 2014; Anglada and Solé, 2016). The stabilized
64 Criegee intermediates (SCIs) can proceed bimolecular reactions with various trace
65 species such as H₂O, NO₂, SO₂, and HCOOH to generate secondary organic aerosol
66 (SOA), thus profoundly influencing air quality, global climate and human health
67 (Osborn and Taatjes, 2015; Khan et al., 2018; Lin and Chao, 2017; Liu et al., 2019;
68 Chhantyal-Pun et al., 2018; Gong and Chen, 2021; Taatjes, 2017).

69 Formic acid (HCOOH), one of the most abundant carboxylic acids, has a
70 significant influence on rainwater acidity in remote areas, where pH reduces by 0.25-
71 0.5 in the presence of HCOOH (Stavrakou et al., 2012; Wang et al., 2020;
72 Chaliyakunnel et al., 2016). It also plays an important role in the formation of cloud
73 condensation nuclei (CCN), indirectly influencing radiative forcing and climate change
74 (Yu, 2000). The primary sources of HCOOH include biomass burning, human activities,
75 tropical and boreal forests, as well as the secondary sources involve the photochemical
76 oxidation of non-methane hydrocarbons, such as ketene-enols, vinyl alcohol, isoprene,
77 and terpenoids (Stavrakou et al., 2012; Wang et al., 2020; Chaliyakunnel et al., 2016;
78 So et al., 2014; Paulot et al., 2011). According to satellite measurements, the production

79 of HCOOH is up to 100-120 Tg yr⁻¹, and the value is expected to increase due to the
80 acceleration of industrialization and urbanization (Stavrakou et al., 2012). Recent
81 kinetics measurements have revealed that the reaction with HCOOH is a more
82 important loss process for SCI than is presently assumed, especially in terrestrial
83 equatorial areas and in high SCI concentration areas (Welz et al., 2014; Chung et al.,
84 2019). The formed hydroperoxide esters have been identified as the low-volatility and
85 high-oxygenated compounds, contributing to the formation and growth of SOA (Welz
86 et al., 2014; Vansco et al., 2021; Sakamoto et al., 2017; Riva et al., 2017).

87 Welz et al. (2014) directly determined the rate coefficients for the reactions of
88 CH₂OO and CH₃CHOO with formic and acetic acid by employing multiplexed
89 photoionization mass spectrometry and cavity-enhanced broadband ultraviolet
90 absorption spectroscopy. They found that the measured rate coefficients are in the
91 excess of $1.0 \times 10^{-10} \text{ cm}^3 \text{ molecule}^{-1} \text{ s}^{-1}$, which are several orders of magnitude greater
92 than those derived from previous experimental studies (Johnson et al., 2001; Tobias and
93 Ziemann, 2001). Sipilä et al. (2014) conducted a competitive reaction kinetics
94 experiment to investigate the reactions of acetone oxide ((CH₃)₂OO) with SO₂,
95 HCOOH and CH₃COOH, and they concluded that the rate coefficients of the (CH₃)₂OO
96 + HCOOH/CH₃OOH reactions are faster than that of the (CH₃)₂OO + SO₂ system by
97 about three times. These high rate coefficients could make the reaction with carboxylic
98 acids a substantial dominant chemical sink for carbonyl oxides in the atmosphere (Welz
99 et al., 2014; Taatjes et al., 2019; Chhantyal-Pun et al., 2017). Quantum chemical
100 calculations show that the reaction of CH₂OO with HCOOH proceeds through a facile
101 transfer of hydrogen atom from the acidic OH group to the terminal oxygen of CH₂OO
102 to form hydroperoxymethyl formate (HPMF) (Long et al., 2009; Vereecken, 2017;
103 Porterfield et al., 2019). Chen et al. (2018) concluded the same by investigating the
104 reactions of various carbonyl oxides with HCOOH that the barrierless 1,4-insertion
105 reaction is the most favorable pathway, and the primary products are hydroperoxide
106 esters. Caravan et al. (2020) employed high-level ab initio CCSD(T)-F12 methods to
107 study the reaction of methyl vinyl ketone oxide (MVK-oxide) with HCOOH, and they

108 found that the barrierless net insertion of MVK-oxide into HCOOH leading to the
109 formation of a functionalized hydroperoxide is dominant over fragmentation to produce
110 an alkoxy radical and OH radicals. Moreover, oligomerization reactions with
111 hydroperoxides and peroxy radicals are identified as one of the dominant loss processes
112 for carbonyl oxides under atmospheric conditions (Sakamoto et al., 2013; Sadezky et
113 al., 2008; Zhao et al., 2015; Chen et al., 2017 and 2019). All the above milestone
114 investigations provide important information for understanding the chemistry of
115 Criegee intermediate in the presence of carboxylic acids. However, to the best of our
116 knowledge, there are few studies on the oligomerization reactions of SCIs with
117 hydroperoxide esters, which are important with regard to organic new particle and cloud
118 condensation nuclei formations. Moreover, the relationship between the reactivity of
119 SCIs and the nature of substituents remains uncertain in the SCIs oligomerization
120 reactions.

121 In the present study, we mainly focus on the oligomerization reaction mechanisms
122 and kinetics of four carbonyl oxides reactions with their respective hydroperoxide esters
123 as well as with HPMF by employing quantum chemical calculations and kinetics
124 modeling methods. For the initiation reactions of carbonyl oxides with formic acid, four
125 kinds of pathways including 1,4 O-H insertion, 1,2 O-H insertion, C-H insertion, and
126 C=O cycloaddition are considered. For the oligomerization reactions of the successive
127 insertion of carbonyl oxides into hydroperoxide esters, two types of reactions involving
128 –OOH and –CH insertions are taken into account. The selected carbonyl oxides,
129 including CH₂OO, *syn*-, *anti*-CH₃CHOO and (CH₃)₂CHOO, are anticipated upon the
130 ozonolysis of ethylene, propylene, and 2,3-dimethyl-2-butene, whereas the
131 hydroperoxide esters are assumed to arise from the bimolecular reactions of carbonyl
132 oxides with formic acid in the atmosphere.

133 **2. Computational details**

134 **2.1 Electronic structure and energy calculations**

135 The geometries of all stationary points, including reactants (R), intermediates (IM),
136 transition states (TS), and products (P), are optimized at the M06-2X/6-311+G(2df,2p)

137 level of theory, since the M06-2X functional has the reliable performance for predicting
138 thermochemistry, kinetics and hydrogen bonding interactions (Zhao and Truhlar, 2008).
139 Harmonic vibrational frequencies are performed at the same level to verify the nature
140 of transition state (NIMAG = 1) and minimum (NIMAG = 0), and to provide zero-point
141 vibrational energy (ZPVE) and Gibbs free energies corrections (G_{corr}), which are scaled
142 by a factor of 0.98 (Alecú et al., 2010). Intrinsic reaction coordinate (IRC) calculations
143 are carried out to verify that each transition state is connected to the desired reactant
144 and product (Fukui, 1981). The single point energy (SPE) calculations are performed
145 at the M06-2X/ma-TZVP level of theory based on the M06-2X/6-311+G(2df,2p)
146 optimized geometries. Moreover, the basis set superposition error (BSSE) is performed
147 by using the counterpoise method proposed by Boys and Bernardi (1970) to evaluate
148 the stability of the pre-reactive complex (RC). Herein, the Gibbs free energy (G) is
149 defined as the sum of SPE and Gibbs correction ($G = E + G_{\text{corr}}$). Electronic energy (ΔE^\ddagger)
150 and Gibbs free energy (ΔG^\ddagger) barriers are defined as the difference in energy between a
151 TS and a RC ($\Delta E^\ddagger = E_{\text{TS}} - E_{\text{RC}}$ and $\Delta G^\ddagger = G_{\text{TS}} - G_{\text{RC}}$). Reaction Gibbs free energy (ΔG)
152 is defined as the difference in energy between a P and a R ($\Delta G = G_{\text{P}} - G_{\text{R}}$).

153 To further assess the reliability of the selected M06-2X/ma-TZVP method for SPE
154 calculations, the single point energies of all stationary points involved in the initiation
155 reactions of distinct SCIs with HCOOH are recalculated at the high-accuracy
156 CCSD(T)/6-311+G(2df,2p) and QCISD(T)/6-311+G(2df,2p) levels of theory. The
157 calculated results are summarized in Table S1. This table shows that the ΔE^\ddagger and ΔG^\ddagger
158 obtained using the QCISD(T) method are in excellent agreement with those obtained
159 using the CCSD(T) approach. It is therefore that the energies obtained using the
160 CCSD(T) method are used as the benchmark for comparison. The mean absolute
161 deviations (MAD) of ΔE^\ddagger and ΔG^\ddagger between the CCSD(T) and M06-2X methods are
162 0.43 and 0.41 kcal mol⁻¹, respectively; the largest deviations of ΔE^\ddagger and ΔG^\ddagger are 1.0
163 and 1.1 kcal mol⁻¹, respectively. These results reveal that the energies obtained using
164 the M06-2X method are close to those obtained using the CCSD(T) approach.
165 Therefore, the M06-2X/ma-TZVP method is suitable to investigate the SCIs

166 oligomerization reactions. In the following discussion, the energies are applied in terms
167 of Gibbs free energy to describe the reaction mechanism unless otherwise stated. All
168 electronic structure calculations are carried out by using Gaussian 09 program (Frisch
169 et al., 2009). The Multiwfn program and Visual molecular dynamics (VMD) are utilized
170 to analysis and visualize the molecular orbitals of the relevant species (Lu and Chen,
171 2012).

172 **2.2 Kinetics calculations**

173 The rate coefficients for the barrierless reactions are determined by employing the
174 inverse Laplace transformation (ILT) method. The ILT calculations are performed with
175 the MESMER 6.0 program (Glowacki et al., 2012). In the ILT treatment, the rotational
176 constants, vibrational frequencies, molecular weights, energies and other input
177 parameters are obtained from the M06-2X/6-311+G(2df,2p) or M06-2X/ma-TZVP
178 methods. For the barrierless reaction of 1,4 O-H insertion of SCIs into HCOOH, SCIs
179 and HCOOH are assigned as the deficient and excess reactants, respectively. The
180 concentration of HCOOH is given a value of 5.0×10^{10} molecules cm^{-3} in the simulation,
181 which is taken from the typical concentration of HCOOH in the tropical forest
182 environments (Vereecken et al., 2012). N_2 is applied as the buffer gas. A single
183 exponential down model is employed to simulate the collision transfer ($\langle \Delta E \rangle_{\text{down}} = 200$
184 cm^{-1}). The collisional Lennard-Jones parameters are estimated with the empirical
185 formula described by Gilbert and Smith (1990).

186 The rate coefficients for the bimolecular reactions with the tight transition states
187 are calculated by using the canonical transition state theory (CTST) along with one-
188 dimensional asymmetric Eckart tunneling correction (Truhlar et al., 1996; Eckart, 1930).
189 The CTST/Eckart calculations are performed with the KiSTheLP 2019 program
190 (Canneaux et al., 2013). As shown in Fig. 1, the entrance pathway Entry2 of $\text{R}_1\text{R}_2\text{COO}$
191 reaction with HCOOH consists of two steps: (i) an intermediate IMent2 is formed via
192 a barrierless process; (ii) then, it rearranges to the product Pent2 through a tight
193 transition state TSent2. The whole reaction process can be described as Eq. (1):



195 Assuming the rapid equilibrium is established between the IMent2 and reactants.
 196 According to the steady-state approximation (SSA), the total rate coefficient is
 197 approximately expressed as Eq. (2) (Zhang et al., 2012):

198
$$k_{\text{tot}} = \frac{k_1}{k_{-1} + k_2} k_2 \approx \frac{k_1}{k_{-1}} k_2 = K_{\text{eq}} k_2 \quad (2)$$

199 The equilibrium constant K_{eq} is written as Eq. (3):

200
$$K_{\text{eq}} = \sigma \frac{Q_{\text{IM}}(T)}{Q_{\text{R1}}(T)Q_{\text{R2}}(T)} \exp\left(\frac{G_{\text{R}} - G_{\text{IM}}}{RT}\right) \quad (3)$$

201 where σ refers to reaction symmetry number, $Q_{\text{IM}}(T)$, $Q_{\text{R1}}(T)$ and $Q_{\text{R2}}(T)$ denote
 202 the partition functions of intermediate, reactants R1 and R2, which are equal to the
 203 multiplication of translational, rotational, vibrational and electronic partition functions
 204 ($Q = Q_{\text{rot}}Q_{\text{vib}}Q_{\text{trans}}Q_{\text{elec}}$) (Mendes et al., 2014), T is the temperature in Kelvin, R is the
 205 ideal gas constant, G_{R} and G_{IM} are the total Gibbs free energies of reactant and
 206 intermediate, respectively.

207 **3. Results and discussion**

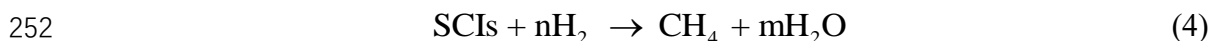
208 **3.1 Initiation reactions of distinct SCIs with HCOOH**

209 The reaction with HCOOH is one of the dominant loss processes for SCIs and is
 210 expected to trigger the formation of SOA in the atmosphere (Chhantyal-Pun et al., 2018;
 211 Cabezas and Endo, 2020; Zhao et al., 2018; Zhou et al., 2019). The potential energy
 212 surface (PES) of distinct SCIs (CH_2OO , *syn*-, *anti*- CH_3CHOO and $(\text{CH}_3)_2\text{COO}$)
 213 reactions with HCOOH is drawn in Fig. 1. The geometries of all stationary points are
 214 displayed in Fig. S1. The relative free energy of each stationary point and free energy
 215 barrier (ΔG^\ddagger) of each elementary reaction are summarized in Table 1. As shown in Fig.
 216 1, the bimolecular reaction of distinct SCIs with HCOOH proceeds via four possible
 217 pathways, namely (1) 1,4 O-H insertion (Entry 1), (2) 1,2 O-H insertion (Entry 2), (3)
 218 C-H insertion (Entry 3), and (4) C=O cycloaddition (Entry 4). For Entry 1, the addition
 219 reaction of CH_2OO with HCOOH proceeds through the 1,4 O-H insertion of CH_2OO

220 into HCOOH to form a hydroperoxide ester HC(O)O-CH₂OO-H with a exoergicity of
 221 37.6 kcal·mol⁻¹. The formation of HC(O)O-CH₂OO-H is obtained through a concerted
 222 process of O₂-H₂ bond breaking in the HCOOH and O₄-H₂ and C₂-O₁ bonds forming.
 223 Despite an attempt by various methods, the corresponding transition state is still not
 224 located in the effort of optimization. To further validate the barrierless process of 1,4
 225 O-H insertion reaction, a relaxed scan over the O₄-H₂ and C₂-O₁ bonds is performed at
 226 the M06-2X/6-311+G(2df,2p) level of theory. The scans start from the optimized
 227 structure of the adduct product HC(O)O-CH₂OO-H, and the O₄-H₂ and C₂-O₁ bond
 228 length are then increased in steps of 0.10 Å. The relaxed scan energy profiles are
 229 presented in Fig. S2. As seen in Fig. S2a, the relative energy of the minimum energy
 230 path from reactant to product decreases monotonically when the bond length of O₄-H₂
 231 and C₂-O₁ bonds decreases, suggesting that the transition state is not exist in the 1,4 O-
 232 H insertion reaction of CH₂OO with HCOOH. Similar conclusion is also obtained from
 233 the relaxed scan energy profiles for the HCOOH + *anti*-CH₃CHOO, HCOOH + *syn*-
 234 CH₃CHOO and HCOOH + (CH₃)₂COO (Fig. S2b-d) reactions that 1,4 O-H insertion
 235 reactions are barrierless. This conclusion is further supported by the analogous reaction
 236 systems that 1,4 O-H insertion reactions of carbonyl oxides with carboxylic acids are a
 237 barrierless process including concerted hydrogen atom transfer and new C-O bond
 238 formation (Chhantyal-Pun et al., 2017; Long et al., 2009; Vereecken, 2017; Cabezas
 239 and Endo, 2019; Lin et al., 2019).

240 The exothermicity of 1,4 O-H insertion reactions of distinct SCIs with HCOOH is
 241 assessed by the reaction enthalpy ($\Delta_r H_{298}^{\circ}$), which is defined as the difference between
 242 the enthalpies of formation ($\Delta_f H_{298}^{\circ}$) of the products and reactants
 243 ($\Delta_r H_{298}^{\circ} = \sum_{\text{products}} \Delta_f H_{298}^{\circ} - \sum_{\text{reactants}} \Delta_f H_{298}^{\circ}$). To the best of our knowledge, there are no literature
 244 values available on the enthalpies of formation of carbonyl oxides and hydroperoxide
 245 esters except the simplest carbonyl oxide CH₂OO. Therefore, the isodesmic reaction
 246 method is adopted to obtain the enthalpies of formation, and the results are listed in
 247 Table S2. An isodesmic reaction is a hypothetical reaction, in which the type of

248 chemical bonds in the reactants is the similar as that of chemical bonds in the products.
249 The following isodesmic reaction is constructed because the experimental values of H₂,
250 CH₄ and H₂O are available ($\Delta_f H_{298}^\circ(\text{H}_2) = 0.00 \text{ kcal}\cdot\text{mol}^{-1}$; $\Delta_f H_{298}^\circ(\text{CH}_4) = -17.82$
251 $\text{kcal}\cdot\text{mol}^{-1}$; $\Delta_f H_{298}^\circ(\text{H}_2\text{O}) = -57.79 \text{ kcal}\cdot\text{mol}^{-1}$).



253 As seen in Table S2, the enthalpy of formation of CH₂OO is calculated to be 23.23
254 $\text{kcal}\cdot\text{mol}^{-1}$, which is in good agreement with the available literature values (Chen et al.,
255 2016; Karton et al., 2013). This result implies that the theoretical method employed
256 herein is reasonable to predict the thermochemical parameters. The enthalpies of
257 formation of carbonyl oxides and hydroperoxide esters significantly decrease with
258 increasing the number of methyl groups. Notably, the decreased values in the enthalpies
259 of formation of carbonyl oxides are greater than those of hydroperoxide esters under
260 the condition of the same number of methyl groups. For example, the enthalpy of
261 formation of *anti*-CH₃CHOO decreases by 12.95 $\text{kcal}\cdot\text{mol}^{-1}$ compared to the enthalpy
262 of formation of CH₂OO, and the enthalpy of formation of Pent1b decreases by 12.12
263 $\text{kcal}\cdot\text{mol}^{-1}$ compared to the enthalpy of formation of Pent1a. The reaction enthalpies
264 decrease in the order of $-44.69 (\text{CH}_2\text{OO} + \text{HCOOH} \rightarrow \text{Pent1a}) < -43.86 (\textit{anti}$ -
265 $\text{CH}_3\text{CHOO} + \text{HCOOH} \rightarrow \text{Pent1b}) < -38.13 (\textit{syn}$ -CH₃CHOO + HCOOH → Pent1c) < -
266 $37.12 \text{ kcal}\cdot\text{mol}^{-1} ((\text{CH}_3)_2\text{COO} + \text{HCOOH} \rightarrow \text{Pent1d})$, indicating that the reaction
267 enthalpies are highly dependent on the number and location of methyl groups. The trend
268 in reaction enthalpies is consistent with the trend in the enthalpies of formation of
269 carbonyl oxides. The reason might be attributed to the decreased values in the enthalpies
270 of formation of carbonyl oxides greater than those of hydroperoxide esters under the
271 condition of the same number of methyl groups.

272 For Entry 2, each addition reaction starts with the formation of a pre-reactive
273 hydrogen bonded complex IMent2 in the entrance channel. Then it immediately
274 converts into product Pent2 through the 1,2 O-H insertion transition state. The
275 formation of Pent2 is obtained via a concerted process of O₂-H₂ bond rupture in the

276 HCOOH and O₄-H₂ and C₂-O₂ bonds forming. The reaction barrier ΔG^\ddagger increases in
277 the order of 10.0 (CH₂OO) < 13.0 (*anti*-CH₃CHOO) < 14.6 (*syn*-CH₃CHOO) \approx 14.4
278 ((CH₃)₂COO) kcal·mol⁻¹, suggesting that the parent CH₂OO + HCOOH reaction is
279 favored kinetically. Compared with the barrier of the parent system, the barrier
280 increases by 3.0 kcal·mol⁻¹ when a methyl substitution occurs at the R₁ position, and
281 the barrier increases by \sim 5 kcal·mol⁻¹ when a methyl group is introduced at the R₂
282 position and dimethyl substituent. The aforementioned result implies that the methyl-
283 substituted CH₂OO hinders the 1,2 O-H insertion of carbonyl oxides into formic acid.
284 Notably, the exothermicity decreases significantly as the number of methyl group is
285 increased. The products Pent1 and Pent2 formed from Entry 1 and 2 are two
286 conformations that differ in the orientation of the -C(O)H moiety over the -OOH group.
287 The calculated result shows that Pent1 is more stable than Pent2 in energy due to the
288 existence of intramolecular hydrogen bond between hydrogen atom of -OOH group
289 and carbonyl oxygen atom.

290 For Entry 3, the addition reaction begins with the formation of a pre-reactive
291 complex IMent3 in the entrance channel, and then it surmounts a barrier to reaction.
292 However, the barriers of C-H insertion reactions are significantly high (21.8-27.6
293 kcal·mol⁻¹), such that they are of less importance in the atmosphere. The high reaction
294 barriers might be attributed to the large bond dissociation energy (BDE) of C-H bond
295 in the formic acid. For Entry 4, the addition reaction proceeds through a cyclization
296 process of C₂-O₁ and O₄-C₁ bond forming to produce a five-membered ring compound
297 Pent4. The barrier of C=O cycloaddition reaction in the CH₂OO + HCOOH reaction is
298 5.8 kcal·mol⁻¹, which is lower than that of the corresponding channels in Entry 2 and
299 Entry 3 by 4.2 and 16.0 kcal·mol⁻¹, respectively. The result reveals that the C=O
300 cycloaddition reaction is feasible kinetically. A similar conclusion is also obtained from
301 the reactions of HCOOH with *syn*-, *anti*-CH₃CHOO and (CH₃)₂COO that the C=O
302 cycloaddition reactions are favored over 1,2 O-H and C-H insertion reactions.

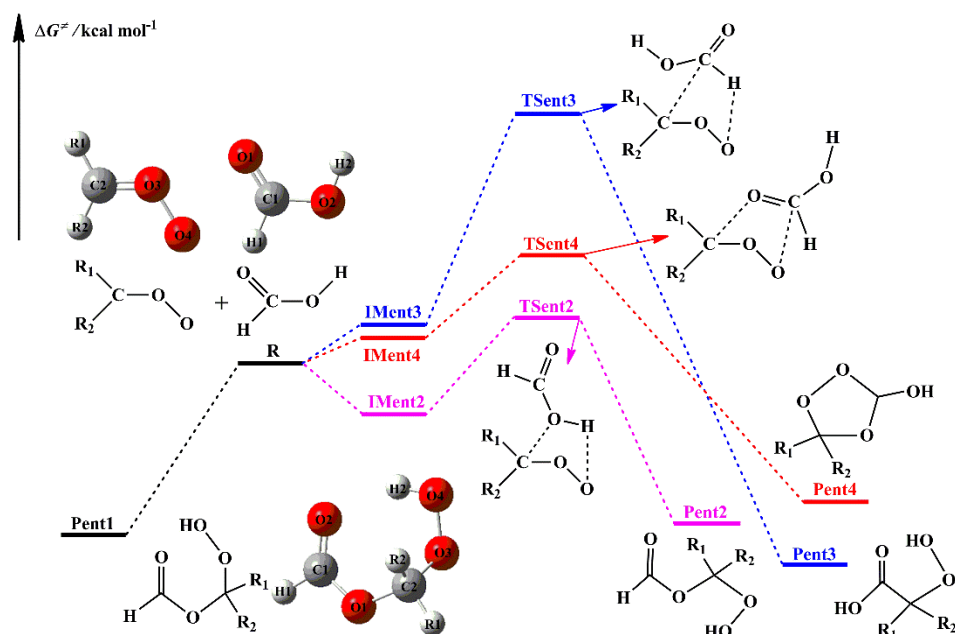
303 The rate coefficients of each elementary pathway included in the initiation
304 reactions of distinct SCIs with HCOOH are calculated in the temperature range of 273-

305 400 K, as listed in Table S3-S6. As shown in Table S3, the total rate coefficients $k_{\text{tot-}}$
306 CH_2OO of CH_2OO reaction with HCOOH are in excess of $1.0 \times 10^{-10} \text{ cm}^3 \text{ molecule}^{-1} \text{ s}^{-1}$,
307 and they exhibit a slightly negative temperature dependence in the temperature range
308 studied. $k_{\text{tot-CH}_2\text{OO}}$ is estimated to be $1.4 \times 10^{-10} \text{ cm}^3 \text{ molecule}^{-1} \text{ s}^{-1}$ at 298 K, which is in
309 good agreement with the experimental values reported by Welz et al. (2014) ($[1.1 \pm 0.1]$
310 $\times 10^{-10}$), Chung et al. (2019) ($[1.4 \pm 0.3] \times 10^{-10}$), and Peltola et al. (2020) ($[1.0 \pm 0.03]$
311 $\times 10^{-10}$). $k(\text{TS}_{\text{ent}1})$ is approximately equal to $k_{\text{tot-CH}_2\text{OO}}$ in the whole temperature range,
312 and it decreases in the range of 1.7×10^{-10} (273 K) to 1.2×10^{-10} (400 K) $\text{cm}^3 \text{ molecule}^{-}$
313 $^1 \text{ s}^{-1}$ with increasing temperature. $k(\text{TS}_{\text{ent}1})$ is several orders of magnitude greater than
314 $k(\text{TS}_{\text{ent}2})$, $k(\text{TS}_{\text{ent}3})$ and $k(\text{TS}_{\text{ent}4})$ over the temperature range from 273 to 400 K. The
315 result again shows that the barrierless 1,4 O-H insertion reaction is predominant. The
316 calculated $K_{\text{eq-ent}2}$, $k_{2\text{-ent}2}$, and $k(\text{TS}_{\text{ent}2})$ ($k(\text{TS}_{\text{ent}2}) = K_{\text{eq-ent}2} \times k_{2\text{-ent}2}$) in Entry 2 are listed
317 in Table S7. This table shows that $K_{\text{eq-ent}2}$ significantly decreases with increasing
318 temperature, and $k_{2\text{-ent}2}$ increases as the temperature is increased. However, the
319 decreased value in $K_{\text{eq-ent}2}$ is greater than the increased value in $k_{2\text{-ent}2}$ under the same
320 temperature range. For example, $K_{\text{eq-ent}2}$ decreases by a factor of 6.3 and $k_{2\text{-ent}2}$ increases
321 by a factor of 2.9 at 298 K compared with the values of $K_{\text{eq-ent}2}$ and $k_{2\text{-ent}2}$ at 273 K. It is
322 therefore that $k(\text{TS}_{\text{ent}2})$ decreases with the temperature increasing. Similar conclusion
323 is also obtained from the results of the rate coefficients in Entry 4 that $k(\text{TS}_{\text{ent}4})$ exhibits
324 a negative temperature dependence in the temperature range studied (Table S8). The
325 aforementioned results imply that $k(\text{TS}_{\text{ent}2})$ and $k(\text{TS}_{\text{ent}4})$ are mediated by the pre-
326 reactive complexes $\text{IMent}2$ and $\text{IMent}4$ in the Entry 2 and 4. It should be noted that
327 although the barrier of Entry 2 is $4.2 \text{ kcal}\cdot\text{mol}^{-1}$ higher than that of Entry 4, $k(\text{TS}_{\text{ent}2})$ is
328 merely about 1-2 fold smaller than $k(\text{TS}_{\text{ent}4})$. The reason is ascribed to the fact that the
329 $\text{C}=\text{O}$ cycloaddition reaction is entropically unfavorable (Vereecken, 2017).

330 Equivalent to the case of CH_2OO reaction with HCOOH , the rate coefficient of
331 each elementary pathway involved in the *anti*- $\text{CH}_3\text{CHOO} + \text{HCOOH}$ reaction also
332 decreases with the temperature increasing (Table S4). This table shows that Entry 1 is
333 kinetically favored over Entry 2, 3 and 4, and Entry 2 is competitive with Entry 4 in the

334 range 273-400 K. Similar conclusion is also obtained from the results of the rate
335 coefficients for the reactions of *syn*-CH₃CHOO and (CH₃)₂COO with HCOOH that
336 Entry 1 is the dominant pathway (Table S5-S6). It deserves mentioning that the
337 competition of Entry 2 is significantly greater than that of Entry 4 in the *syn*-CH₃CHOO
338 + HCOOH and (CH₃)₂COO + HCOOH systems. Based on the above discussions, it can
339 be concluded that the relative importance of different pathways is highly dependent on
340 the number and location of methyl substituents in the carbonyl oxides. Notably, the rate
341 coefficient of each elementary pathway included in the *anti*-CH₃CHOO + HCOOH
342 reaction is several orders of magnitude greater than that of the corresponding channel
343 involved in the other SCIs + HCOOH systems. It is because that *anti*-CH₃CHOO is
344 substantially more reactive toward HCOOH than other SCIs. Similar phenomenon has
345 also observed from the reactivity of *anti*-CH₃CHOO toward water and SO₂ (Taatjes et
346 al., 2013; Long et al., 2016; Huang et al., 2015; Cabezas and Endo, 2018). At ambient
347 temperature, the total rate coefficients of HCOOH reactions with *anti*-CH₃CHOO, *syn*-
348 CH₃CHOO and (CH₃)₂COO are estimated to be 5.9, 2.7 and 4.8 × 10⁻¹⁰ cm³ molecule⁻¹
349 s⁻¹, respectively, which are consistent with the prior experimental measurements of 5
350 ± 3, 2.5 ± 0.3 and 4.5 × 10⁻¹⁰ cm³ molecule⁻¹ s⁻¹ (Welz et al., 2014; Chung et al., 2019;
351 Sipilä et al., 2014).

352 In summary, the barrierless 1,4 O-H insertion reaction is the dominant pathway in
353 the initiation reactions of distinct SCIs with HCOOH. This conclusion is consistent with
354 the recent experimental results derived from the reactions of formic acid with
355 methacrolein oxide (MACR-OO) and methyl vinyl ketone oxide (MVK-OO) that the
356 1,4-addition mechanism is energetically favorable (Vansco et al., 2021; Caravan et al.,
357 2020). Therefore, in the present study, the adduct products Pent1 formed from the
358 barrierless 1,4 O-H insertion of carbonyl oxides into HCOOH are selected as the model
359 compounds to investigate the oligomerization reaction mechanisms of carbonyl oxides
360 reactions with hydroperoxide esters.



361

362 **Figure 1.** Schematic PES for the possible entrance pathways of the initiation reactions of HCOOH
 363 with various SCIs (black, pink, blue, and red lines represent 1,4 O-H insertion, 1,2 O-H insertion,
 364 C-H insertion, and C=O cycloaddition reactions, respectively)

365 **Table 1** Relative free energies of stationary points and free-energy barriers (ΔG^\ddagger) at 298 K in kcal
 366 mol⁻¹ for the various SCIs (R₁R₂COO, R₁, R₂=H, CH₃) reactions with HCOOH calculated at the
 367 M06-2X/ma-TZVP//M06-2X/6-311+G(2df,2p) level of theory

Entry	R1	R2	IMent	TSent	Pent	ΔG^\ddagger
1	H	H	–	–	-37.6	–
	CH ₃	H	–	–	-34.0	–
	H	CH ₃	–	–	-29.8	–
	CH ₃	CH ₃	–	–	-25.6	–
2	H	H	-3.1	6.9	-37.3	10.0
	CH ₃	H	-11.0	2.0	-33.7	13.0
	H	CH ₃	-6.6	8.0	-29.1	14.6
	CH ₃	CH ₃	-8.8	5.6	-24.9	14.4
3	H	H	3.4	25.2	-46.9	21.8
	CH ₃	H	1.8	24.0	-41.5	22.2
	H	CH ₃	3.0	30.6	-37.6	27.6
	CH ₃	CH ₃	1.9	29.5	-33.0	27.6
4	H	H	3.4	9.2	-31.7	5.8
	CH ₃	H	2.2	7.8	-29.4	5.6
	H	CH ₃	3.5	14.6	-25.3	11.1
	CH ₃	CH ₃	3.0	13.2	-22.9	10.2

368 **3.2. The reactions of distinct SCIs with their respective hydroperoxide**

369 **esters**

370 The formed hydroperoxide ester has two possible unimolecular decay pathways.
371 The first is the direct O-O bond rupture resulting in the formation of oxylmethylformate
372 and OH radicals (Vereecken, 2017). The second is the $-OH$ fragment binding to
373 adjacent hydrogen atom leading to the formation of anhydride and H_2O (Aplincourt and
374 Ruiz-López, 2000; Neeb et al., 1998). However, the barriers of these two unimolecular
375 reactions are extremely high, such that they are of less importance in the atmosphere.
376 The formed hydroperoxide ester possess $-OOH$ and $-OC(O)H$ groups, both of them
377 can serve as the reactive moieties to react with carbonyl oxides giving rise to the
378 formation of oligomers. In the present study, we mainly consider two types of pathways:
379 (a) $-OOH$ insertion and (b) $-CH$ insertion, while the $C=O$ cycloaddition reaction is not
380 taken into account because it is entropically unfavorable (Vereecken, 2017; Lin, et al.,
381 2019). The aforementioned reactions are discussed in detail in the following
382 subsections.

383 **3.2.1 The reactions of $2CH_2OO$ with Pent1a**

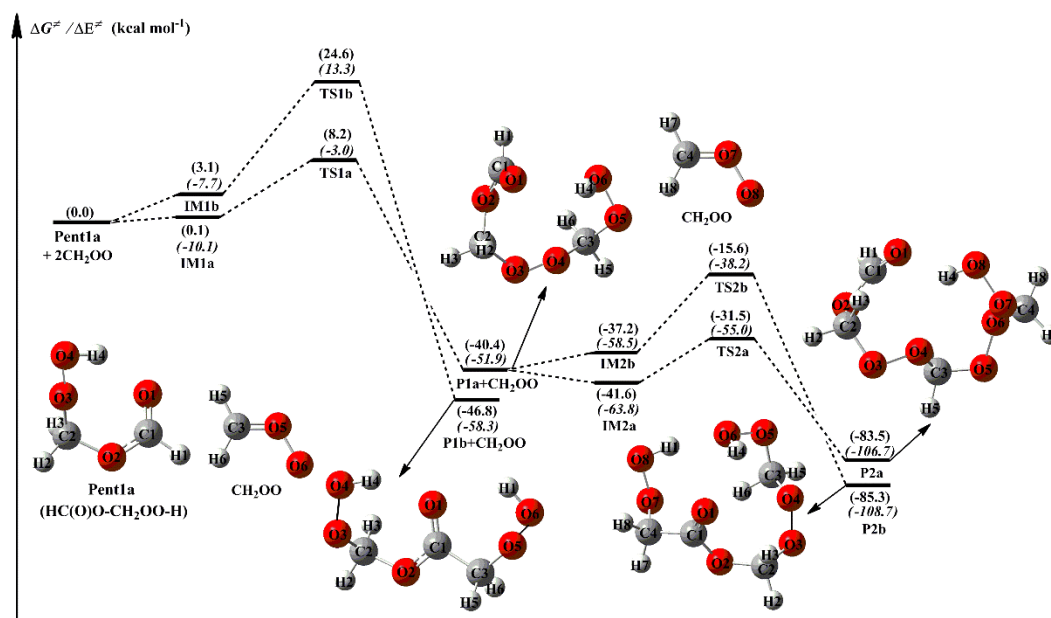
384 The simplest carbonyl oxide, CH_2OO , originates from the reaction of all terminal
385 alkenes with ozone (ozonolysis) in the atmosphere (Lin and Chao, 2017). The reaction
386 with $HCOOH$ is expected to be one of the dominant loss processes for CH_2OO , and the
387 main product is Pent1a (also called as HPMF) (Welz et al., 2014; Cabezas and Endo,
388 2019). A schematic PES for the addition reaction $2CH_2OO + Pent1a$ is drawn in Fig. 2,
389 and the optimized geometries of all stationary points are displayed in Fig. S3. As seen
390 in Fig. 2, the successive insertion of CH_2OO into Pent1a eventually leads to the
391 formation of oligomers P2a and P2b composed of CH_2OO as the repeat unit. These
392 oligomerization reactions are strongly exothermic and spontaneous ($> 83 \text{ kcal}\cdot\text{mol}^{-1}$),
393 implying that they are feasible thermodynamically.

394 The addition reaction $2CH_2OO + Pent1a$ initially proceeds through two possible
395 pathways, namely (1) $-OOH$ insertion reaction R1a, and (2) $-CH$ insertion reaction R1b.
396 For the $-OOH$ insertion reaction R1a, the pre-reactive intermediate IM1a with a seven-
397 membered ring structure is formed in the entrance channel, which is stabilized by the
398 hydrogen bond interactions between the H_4 atom of Pent1a and the O_6 atom of CH_2OO

399 ($D_{(O_6-H_4)} = 1.706 \text{ \AA}$), and between the H_6 atom of CH_2OO and the O_3 atom of Pent1a
400 ($D_{(O_3-H_6)} = 2.115 \text{ \AA}$). Then IM1a converts into P1a ($C_3H_6O_6$, $HC(O)O-(CH_2OO)_2-H$)
401 via a concerted process of O_4-H_4 bond breaking in the Pent1a and O_4-C_3 and H_4-O_6
402 bonds forming with a barrier of $8.1 \text{ kcal}\cdot\text{mol}^{-1}$. For the $-CH$ insertion reaction R1b, the
403 pre-reactive intermediate IM1b with a seven-membered ring structure is formed in the
404 entrance channel, which is stabilized by the van der Waals (vdW) interactions between
405 the O_3 atom of Pent1a and the C_3 atom of CH_2OO ($D_{(O_3-C_3)} = 2.602 \text{ \AA}$), and between
406 the O_6 atom of CH_2OO and the C_1 atom of Pent1a ($D_{(O_6-C_1)} = 2.608 \text{ \AA}$). Due to the
407 absence of hydrogen bond in IM1b, the energy of IM1b is lower than that of IM1a by
408 $3.0 \text{ kcal}\cdot\text{mol}^{-1}$. IM1b transforms into P1b ($C_3H_6O_6$, $HO_2CH_2OC(O)CH_2OOH$) via a
409 concerted process of C_1-H_1 bond breaking in the Pent1a and C_1-C_3 and H_1-O_6 bonds
410 forming with a barrier of $21.5 \text{ kcal}\cdot\text{mol}^{-1}$. By comparing the barriers of R1a and R1b, it
411 can be concluded that the $-OOH$ insertion reaction is favored over the $-CH$ insertion
412 reaction. The high reaction barrier of R1b is attributed to the large bond dissociation
413 energy (BDE) of C-H bond in the Pent1a. To further insight into the reaction mechanism
414 of R1a, the natural bond orbital (NBO) analysis of the donor-accepter orbitals involved
415 in the TS1a is performed using the M06-2X wave function. The possible donor-accepter
416 interactions are estimated by using the second order perturbation theory. As illustrated
417 in Fig. S4, the strong interactions are identified as the interaction of the lone pair orbital
418 of O_6 atom and the antibonding orbital of O_4-H_4 bond, and the interaction of the lone
419 pair orbital of O_4 atom and the antibonding orbital of C_3-O_5 bond.

420 Similarly, the addition reaction $CH_2OO + P1a$ proceeds through the formation of
421 the pre-reactive intermediates IM2a and IM2b in the entrance channel, which are
422 stabilized by a hydrogen bond between the terminal oxygen atom of CH_2OO and the
423 reacting hydrogen atom of P1a, and a van der Waals (vdW) interaction between the
424 central carbon atom of CH_2OO and the carbonyl oxygen atom of P1a. The relative
425 energies of IM2a and IM2b with respect to the separate reactants P1a and CH_2OO are
426 -1.2 and $3.2 \text{ kcal}\cdot\text{mol}^{-1}$, respectively, below the energies of the initial reactants $2CH_2OO$
427 and Pent1a are 41.6 and $37.2 \text{ kcal}\cdot\text{mol}^{-1}$, respectively. Then they immediately transform

428 into the respective products P2a and P2b through the –OOH and –CH insertion
 429 transition states TS2a and TS2b with the barriers of 10.1 and 21.6 kcal·mol⁻¹. This result
 430 again shows that the –OOH insertion reaction is favored kinetically. It deserves
 431 mentioning that the barrier of –OOH insertion reaction increases as the number of
 432 CH₂OO is increased. From the viewpoint of the geometrical parameters of TS2a and
 433 TS2b, the breaking O-H and C-H bonds are elongated by 14.8% and 20.6%,
 434 respectively, with respect to the equilibrium structures of IM2a and IM2b, while the
 435 forming C-O and C-C bond length are 2.013 and 2.264 Å, respectively. The result
 436 reveals that TS2a and TS2b are structurally reactant-like, which are consistent with the
 437 Hammond's hypothesis that the earlier transition states are generally exothermic
 438 (Hammond, 1955).

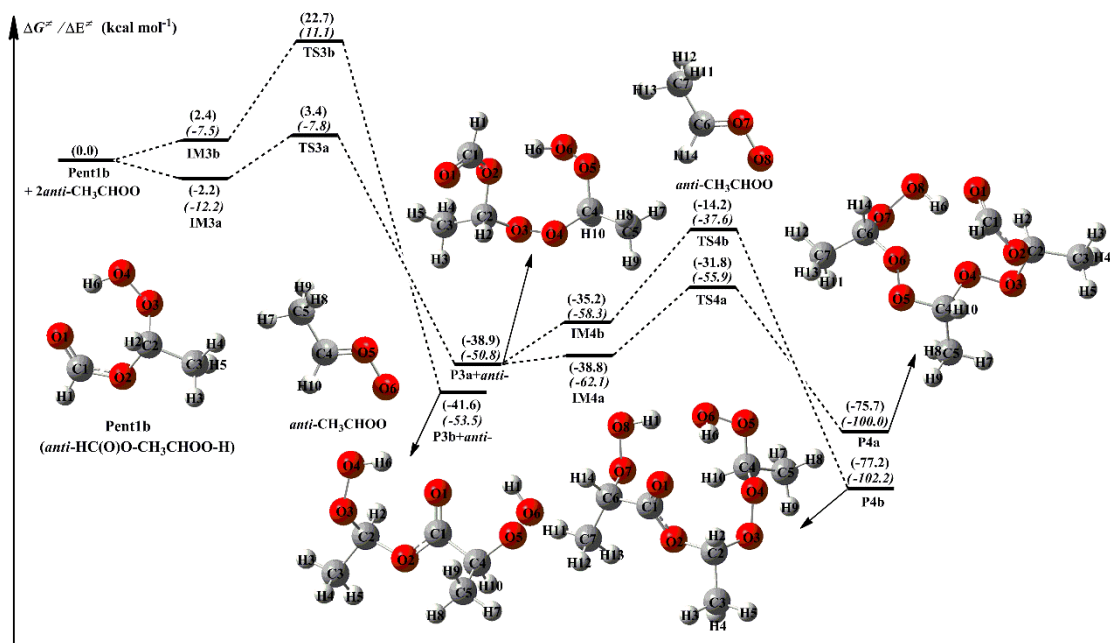


439
 440 **Figure 2.** PES (ΔG and ΔE , in italics) for the $2\text{CH}_2\text{OO} + \text{Pent1a}$ reaction at the M06-2X/ma-
 441 TZVP//M06-2X/6-311+G(2df,2p) level of theory

442 3.2.2 The reactions of *anti*-CH₃CHOO with Pent1b

443 The methyl-substituted CH₂OO has two conformers, *syn*- and *anti*-CH₃CHOO that
 444 distinguish by the orientation of methyl group relative to the terminal oxygen (Taatjes
 445 et al., 2013). *syn*-CH₃CHOO is more stable than *anti*-CH₃CHOO in energy due to the
 446 existence of intramolecular hydrogen bond (Long et al., 2016). The activation enthalpy
 447 of the interconversion between *syn*-CH₃CHOO and *anti*-CH₃CHOO is up to 38.5
 448 kcal·mol⁻¹, implying that they can treat as independent species in the atmosphere (Long

449 et al., 2016; Yin and Takahashi, 2017). A schematic PES for the addition reaction 2*anti*-
450 CH₃CHOO + Pent1b is presented in Fig. 3, and the optimized geometries of all
451 stationary points are shown in Fig. S5. As shown in Fig. 3, the addition reaction 2*anti*-
452 CH₃CHOO + Pent1b proceeds through successive insertion of *anti*-CH₃CHOO into
453 Pent1b leading to the formation of oligomers P4a and P4b that contain *anti*-CH₃CHOO
454 as chain unit. The first *anti*-CH₃CHOO addition reaction begins with the formation of
455 IM3a and IM3b in the entrance channel, which lie -2.2 and 2.4 kcal·mol⁻¹ respectively,
456 with respect to the separate reactants. Then the IM3a and IM3b transform into P3a and
457 P3b via -OOH and -CH insertion transition states TS3a and TS3b with the barriers of
458 5.6 and 20.3 kcal·mol⁻¹. This result shows that the -OOH insertion reaction is more
459 favorable than the -CH insertion pathway. Compared with the barriers of R1a and R1b
460 in the 2CH₂OO + Pent1a reaction, the barriers of R3a and R3b decrease by 2.5 and 1.2
461 kcal·mol⁻¹ when a methyl group is introduced at the *anti*-position. The result reveals
462 that the reactivity of *anti*-CH₃CHOO is substantially higher than that of CH₂OO. This
463 conclusion is further supported by the findings of other studies, which have reported
464 that *anti*-CH₃CHOO is more reactive toward H₂O, SO₂, and H₂O₂ than CH₂OO (Chen
465 et al., 2017; Taatjes et al., 2013; Huang et al., 2015). Similarly, the secondary *anti*-
466 CH₃CHOO addition reaction starts with the formation of IM4a and IM4b in the entrance
467 channel with the 0.1 and 3.7 kcal·mol⁻¹ stability, followed by conversion to the final
468 products P4a and P4b through the -OOH and -CH insertion reactions R4a and R4b.
469 The transition states TS4a and TS4b lie 7.0 and 21.0 kcal·mol⁻¹, respectively, above the
470 energies of the respective intermediates IM4a and IM4b. This result again shows that
471 the -OOH insertion reaction is the most favorable channel, and the barrier increases as
472 the number of *anti*-CH₃CHOO is increased.

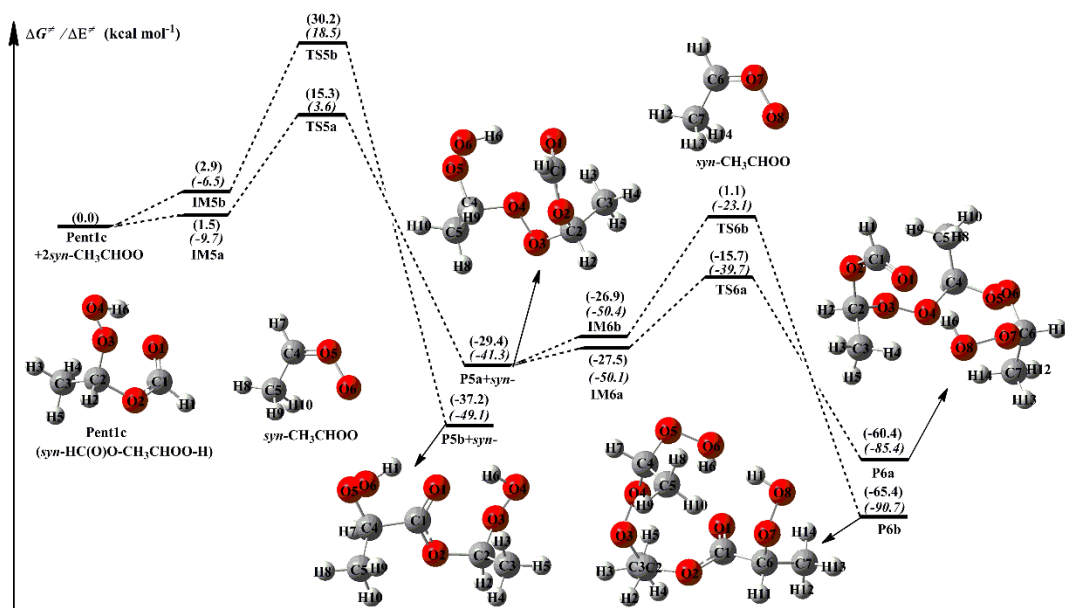


473

474 **Figure 3.** PES (ΔG and ΔE , in italics) for the $2anti\text{-CH}_3\text{CHOO} + \text{Pent1b}$ reaction at the M06-
 475 2X/ma-TZVP//M06-2X/6-311+G(2df,2p) level of theory

476 3.2.3 The reactions of *syn*-CH₃CHOO with Pent1c

477 Equivalent to the $2anti\text{-CH}_3\text{CHOO} + \text{Pent1b}$ reaction, the addition reaction $2syn\text{-}$
 478 $\text{CH}_3\text{CHOO} + \text{Pent1c}$ has similar transformation pathways, and is thus briefly discussed
 479 in the present study. From Fig. 4, it can be seen that the addition reaction $2syn\text{-}$
 480 $\text{CH}_3\text{CHOO} + \text{Pent1c}$ undergoes via successive insertion of *syn*-CH₃CHOO into Pent1c
 481 to form P6a and P6b that involve *syn*-CH₃CHOO as the repeating unit. The most
 482 favorable pathway is that the breakage of O₄-H₆ bond in the -OOH group of Pent1c
 483 occurs simultaneously with the insertion of first *syn*-CH₃CHOO into Pent1c to form
 484 P5a, followed by the insertion of secondary *syn*-CH₃CHOO into P5a to produce P6a.
 485 The barriers of these two -OOH insertion reactions R5a and R6a are 13.8 and 11.8
 486 kcal·mol⁻¹, respectively, which are higher than those of R3a and R4a in the $2anti\text{-}$
 487 $\text{CH}_3\text{CHOO} + \text{Pent1b}$ system by 8.2 and 4.8 kcal·mol⁻¹, respectively. The result reveals
 488 that the reactivity of *syn*-CH₃CHOO is substantially lower than that of *anti*-CH₃CHOO.
 489 Notably, the barrier of the favorable -OOH insertion pathway decreases with increasing
 490 the number of *syn*-CH₃CHOO in the $2syn\text{-CH}_3\text{CHOO} + \text{Pent1c}$ reaction, which is
 491 contrary to the case of the $2\text{CH}_2\text{OO} + \text{Pent1a}$ and $2anti\text{-CH}_3\text{CHOO} + \text{Pent1b}$ reactions.



492

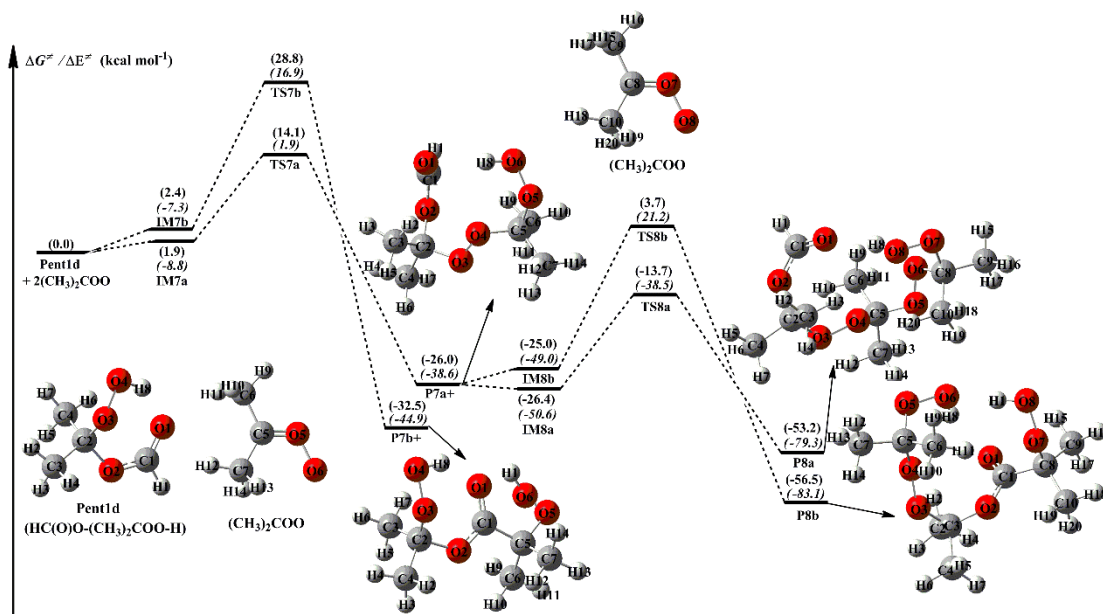
493 **Figure 4.** PES (ΔG and ΔE , in italics) for the $2_{syn}\text{-CH}_3\text{CHOO} + \text{Pent1c}$ reaction at the M06-
 494 2X/ma-TZVP//M06-2X/6-311+G(2df,2p) level of theory

495 3.2.4 The reactions of $2(\text{CH}_3)_2\text{COO}$ with Pent1d

496 The dimethyl-substituted Criegee intermediate, $(\text{CH}_3)_2\text{COO}$, is generated from the
 497 ozonolysis of 2,3-dimethyl-2-butene in the atmosphere (Lester and Klippenstein, 2018;
 498 Drozd et al., 2017; Long et al., 2018). The bimolecular reaction of $(\text{CH}_3)_2\text{COO}$ with
 499 water is not fast enough ($k < 1.5 \times 10^{-16} \text{ cm}^3 \text{ molecule}^{-1} \text{ s}^{-1}$), while the reaction of
 500 $(\text{CH}_3)_2\text{COO}$ with HCOOH has a near gas kinetic limit rate ($k = 5.4 \times 10^{-10} \text{ cm}^3 \text{ molecule}^{-1}$
 501 s^{-1}) (Huang et al., 2015). The result implies that a fraction of $(\text{CH}_3)_2\text{COO}$ may survive
 502 under high humidity environments and react with HCOOH leading to the formation of
 503 hydroperoxide ester Pent1d. A schematic PES for the addition reaction $2(\text{CH}_3)_2\text{COO} +$
 504 Pent1d is plotted in Fig. 5, and the optimized geometries of all stationary points are
 505 shown in Fig. S7.

506 As seen in Fig. 5, the addition reaction $2(\text{CH}_3)_2\text{COO} + \text{Pent1d}$ starts with the
 507 formation of complexes IM7a and IM7b, which lie 1.9 and 2.4 $\text{kcal}\cdot\text{mol}^{-1}$, respectively,
 508 above the energies of the separate reactants. Then they subsequently transform into
 509 products P7a and P7b through the $-\text{OOH}$ and $-\text{CH}$ insertion transition states TS7a and
 510 TS7b with the barriers of 12.2 and 26.4 $\text{kcal}\cdot\text{mol}^{-1}$. This result again shows that the $-\text{OOH}$
 511 insertion reaction is favored over the $-\text{CH}$ insertion pathway. A similar conclusion
 512 is also obtained from the secondary $(\text{CH}_3)_2\text{COO}$ addition reaction that the $-\text{OOH}$

513 insertion reaction is the dominant pathway. It is of interest to compare the barriers of –
 514 OOH insertion reactions in the $(\text{CH}_3)_2\text{COO} + \text{Pent1d}$ system with those of the
 515 analogous reactions in other SCIs + Pent1 reactions. It can be found that the barriers
 516 decrease in the order of *syn*- $\text{CH}_3\text{CHOO} > (\text{CH}_3)_2\text{COO} > \text{CH}_2\text{OO} > \textit{anti}$ - CH_3CHOO in
 517 the first-step SCIs addition reaction, while they become $(\text{CH}_3)_2\text{COO} > \textit{syn}$ - $\text{CH}_3\text{CHOO} >$
 518 $\text{CH}_2\text{OO} > \textit{anti}$ - CH_3CHOO in the second-step SCI addition pathway. The result shows
 519 that the reactivity of SCIs is significantly affected by the number and location of methyl
 520 substituents. A similar conclusion is also obtained from the thermodynamic parameters
 521 that the exothermicity of –OOH insertion reactions significantly decreases with
 522 increasing the number of methyl substituents, and the exothermicity of *anti*-methyl
 523 substituted carbonyl oxide is obviously higher than that of *syn*-methyl substituted
 524 carbonyl oxide.



525
 526 **Figure 5.** PES (ΔG and ΔE , in italics) for the $2(\text{CH}_3)_2\text{COO} + \text{Pent1d}$ reaction at the M06-2X/ma-
 527 TZVP//M06-2X/6-311+G(2df,2p) level of theory.

528 3.3 The reactions of distinct SCIs with Pent1a and implications in 529 atmospheric chemistry

530 To further elucidate the effect of the number and location of methyl substituents
 531 on the reactivity of carbonyl oxides toward hydroperoxide esters, Pent1a (also called as
 532 HPMF) is selected as the model compound since it is the simplest hydroperoxide ester

533 formed from the barrierless reaction of 1,4 O-H insertion of CH₂OO into HCOOH. As
534 mentioned above, –OOH insertion reaction in the oligomerization reactions is the most
535 favorable pathway. Therefore, this type of reaction is merely considered in the reactions
536 of distinct SCIs with Pent1a. The corresponding PES and the optimized geometries of
537 all stationary points are displayed in Figs. 6 and S8, respectively. As seen in Fig. 6, each
538 pathway starts with the formation of a pre-reactive intermediate, and then it overcomes
539 a modest barrier to reaction. The barrier of the reaction of CH₂OO with Pent1a is
540 calculated to be 8.1 kcal·mol⁻¹, which is higher than that of the *anti*-CH₃CHOO +
541 Pent1a reaction by 2.5 kcal·mol⁻¹. The reason of low barrier can be explained by the
542 NPA atomic charges, as presented in Fig. S9. As seen in Fig. S9, the charges of the
543 central carbon atom C₁ and the terminal oxygen atom O₁ of CH₂OO are 0.186e and -
544 0.459e, respectively, indicating that CH₂OO is indeed a zwitterion. The C₁ atom charge
545 becomes more positive (0.393e), while the O₁ atom charge becomes more negative (-
546 0.497e) when a methyl substituent occurs at the *anti*-position. This result suggests that
547 the *anti*-methyl substituent enhances the characteristic of carbonyl oxides zwitterion
548 and reduces the reaction barriers. Compared with the barrier of the CH₂OO + Pent1a
549 reaction, the barriers increase by about 3.0 kcal·mol⁻¹ when a methyl group is
550 introduced at the *syn*-position and dimethyl substituent. Although *syn*-methyl and
551 dimethyl substituent promote the raise of carbonyl oxides zwitterion, the steric
552 hindrance effect and intramolecular hydrogen bond are obviously dominant for *syn*-
553 CH₃CHOO and (CH₃)₂COO, that are not thus conducive to the nucleophilic attack of
554 hydroperoxide esters. It is worth noting that the exothermicity of distinct SCIs reactions
555 with Pent1a obviously decreases as the number of methyl group is increased, and the
556 exothermicity of *anti*-methyl substituent is higher than that of *syn*-methyl substituent.

557 The rate coefficients of distinct SCIs reactions with Pent1a are calculated in the
558 temperature range of 273-400 K as summarized in Table S9. This table shows that the
559 rate coefficients k_{R1a} of the CH₂OO + Pent1a reaction (R1a) decrease in the range of
560 5.0×10^{-11} (273 K) to 5.0×10^{-12} cm³ molecule⁻¹ s⁻¹ (400 K) with increasing temperature.
561 A similar phenomenon is also observed from the rate coefficients of Pent1a reactions

562 with *anti*-CH₃CHOO (R9), *syn*-CH₃CHOO (R10), and (CH₃)₂COO (R11) that they
563 exhibit a slightly negative temperature dependence. k_{R9} is several orders of magnitude
564 greater than k_{R1a} , k_{R10} and k_{R11} in the whole temperature range, suggesting that the
565 bimolecular reaction *anti*-CH₃CHOO + Pent1a (R9) is favored kinetically. Compared
566 with the rate coefficients of R1a, the rate coefficients increase by about one order of
567 magnitude when a methyl substituent occurs at the *anti*-position, whereas the rate
568 coefficients decrease by 1 to 2 orders of magnitude when a methyl group is introduced
569 at the *syn*-position. It should be noted that although the barrier of R10 is nearly identical
570 to that of R11, k_{R10} is 1 to 2 orders of magnitude lower than k_{R11} in the entire temperature
571 range. This is probably because the rate coefficients are mediated by pre-reactive
572 intermediates that IM11 is more stable than IM10 in energy.

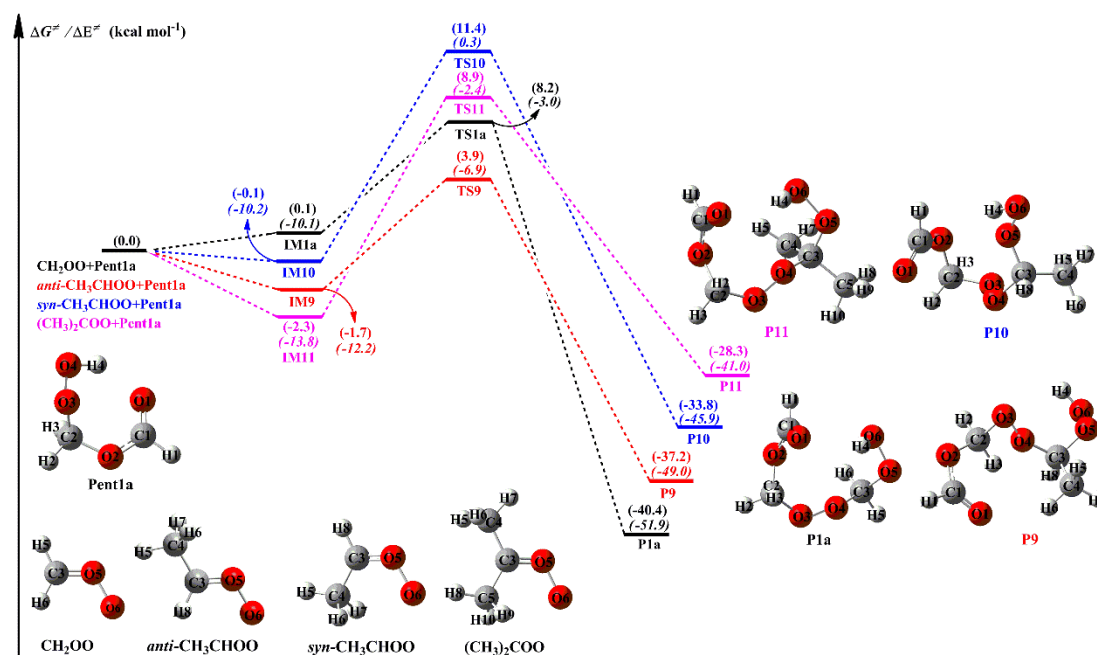
573 It is of interest to assess whether the reactions of distinct SCIs with HPMF can
574 compete well with the losses to reactions with trace species (e.g., H₂O, HCOOH and
575 SO₂), because it is well known that the reactions with trace species are expected to be
576 the dominant chemical sinks for SCIs in the atmosphere (Taatjes et al., 2013; Long et
577 al., 2016). The reported concentrations of coreactant, the rate coefficients k , and the
578 effective pseudo-first-order rate constants ($k_{\text{eff}} = k[\text{coreactant}]$) for distinct SCI
579 reactions with H₂O, HCOOH, SO₂, and HPMF are summarized in Table 2. As seen in
580 Table 2, the rate coefficient of a particular SCI reaction with trace species is strongly
581 dependent on its structure. The methyl group substitution may alter the rate coefficient
582 by several to tens of times. The atmospheric concentrations of H₂O, HCOOH and SO₂
583 in the tropical forest environments are measured to be $3.9\text{-}6.1 \times 10^{17}$, $5.0\text{-}10 \times 10^{10}$, and
584 $1.7\text{-}9.0 \times 10^{10}$ molecules cm⁻³, respectively (Vereecken, 2012). For the reactions of
585 CH₂OO with H₂O, HCOOH, and SO₂, the experimental rate coefficients are determined
586 to be $< 1.5 \times 10^{-15}$, $[1.1 \pm 0.1] \times 10^{-10}$, and $[3.9 \pm 0.7] \times 10^{-11}$ cm³ molecule⁻¹ s⁻¹,
587 respectively (Welz et al., 2012 and 2014; Chao et al., 2015), which translate into
588 $k_{\text{eff(CH}_2\text{OO+H}_2\text{O)}}$, $k_{\text{eff(CH}_2\text{OO+HCOOH)}}$ and $k_{\text{eff(CH}_2\text{OO+SO}_2)}$ of $5.9\text{-}9.2 \times 10^2$, 5.5-11, and 0.7-3.5
589 s⁻¹, respectively. The result reveals that the reaction of CH₂OO with H₂O is the most
590 important bimolecular reaction. $k_{\text{eff(CH}_2\text{OO+HCOOH)}}$ is greater by a factor of 3-8 than

591 $k_{\text{eff}}(\text{CH}_2\text{OO}+\text{SO}_2)$, indicating that the reaction of CH_2OO with HCOOH is favored over
592 reaction with SO_2 . Similar conclusion is also obtained from the results of k_{eff} for the
593 reactions of *anti*- CH_3CHOO , *syn*- CH_3CHOO and $(\text{CH}_3)_2\text{COO}$ with H_2O , HCOOH and
594 SO_2 that SCIs reactions with H_2O are faster than with HCOOH , which, in turn, are
595 faster than with SO_2 .

596 According to the results shown in the Table 2, the room temperature rate
597 coefficient for the reaction of CH_2OO with HPMF is calculated to be $2.7 \times 10^{-11} \text{ cm}^3$
598 $\text{molecule}^{-1} \text{ s}^{-1}$. However, to the best of our knowledge, the atmospheric concentration
599 of HPMF has not been reported up to now. If we assume that the concentration of HPMF
600 is the same as that of HCOOH , $k_{\text{eff}}(\text{CH}_2\text{OO}+\text{HPMF})$ is estimated to be $1.4\text{-}2.7 \text{ s}^{-1}$, which is
601 significantly lower than $k_{\text{eff}}(\text{CH}_2\text{OO}+\text{H}_2\text{O})$ and $k_{\text{eff}}(\text{CH}_2\text{OO}+\text{HCOOH})$. $k_{\text{eff}}(\text{CH}_2\text{OO}+\text{HPMF})$ is nearly
602 identical to $k_{\text{eff}}(\text{CH}_2\text{OO}+\text{SO}_2)$, indicating that the $\text{CH}_2\text{OO} + \text{HPMF}$ reaction is competitive
603 with the $\text{CH}_2\text{OO} + \text{SO}_2$ system. Previous model-measurement studies have estimated
604 the surface-level SCIs concentrations in the range of 1.0×10^4 to 1.0×10^5 molecules
605 cm^{-3} (Khan et al., 2018; Novelli et al., 2017). If we assume that the concentration of
606 HPMF is equal to that of SCIs, $k_{\text{eff}}(\text{CH}_2\text{OO}+\text{HPMF})$ is calculated to be $2.7\text{-}27 \times 10^{-7} \text{ s}^{-1}$,
607 which is several orders of magnitude lower than $k_{\text{eff}}(\text{CH}_2\text{OO}+\text{H}_2\text{O})$, $k_{\text{eff}}(\text{CH}_2\text{OO}+\text{HCOOH})$ and
608 $k_{\text{eff}}(\text{CH}_2\text{OO}+\text{SO}_2)$. This result indicates that the reaction of CH_2OO with HPMF is of less
609 importance. Similar conclusion is also obtained from the reactions of *anti*- CH_3CHOO ,
610 *syn*- CH_3CHOO and $(\text{CH}_3)_2\text{COO}$ with HPMF.

611 To further evaluate the relative importance of the complex SCIs reactions with
612 coreactant, the bimolecular reactions of methyl vinyl ketone oxide (MVK-OO) with
613 H_2O , HCOOH , SO_2 , and HPMF are considered. MVK-OO, formed with 21 to 23%
614 yield from the ozonolysis of isoprene, is a four carbon, asymmetric, resonance-
615 stabilized Criegee intermediate (Barber et al., 2018). MVK-OO has four conformers,
616 *syn-trans*-, *syn-cis*-, *anti-trans*-, and *anti-cis*- as shown in Fig. S10. Herein, *syn* and *anti*
617 refer to the orientation of the $-\text{CH}_3$ group relative to the terminal oxygen of MVK-OO,
618 whereas *cis* and *trans* refer to the orientation of the $\text{C}_8=\text{C}_9$ bond relative to the $\text{C}_1=\text{O}_2$
619 bond. According to the results shown in the Fig. S10, the lowest-energy conformer is

620 *syn-trans*-MVK-OO, which is lower than *syn-cis*-, *anti-trans*-, and *anti-cis*-MVK-OO
 621 by 1.42, 2.43 and 2.69 kcal·mol⁻¹, respectively. Therefore, the lowest-energy conformer
 622 *syn-trans*-MVK-OO is selected as the model compound to study its bimolecular
 623 reactions. As shown in Table 2, the rate coefficient of H₂O reaction with *syn-trans*-
 624 MVK-OO is lower than with other SCIs by 2 to 3 orders of magnitude. The reason is
 625 likely to be that the existence of methyl and vinyl groups hinders the occurrence of
 626 bimolecular reaction with water vapour. Consequently, a fraction of *syn-trans*-MVK-
 627 OO may survive in the presence of water vapour and react with other species. $k_{\text{eff}}(\text{MVK-}$
 628 $\text{OO}+\text{H}_2\text{O})$ is nearly identical to $k_{\text{eff}}(\text{MVK-OO}+\text{HCOOH})$, which is greater than $k_{\text{eff}}(\text{MVK-OO}+\text{SO}_2)$
 629 and $k_{\text{eff}}(\text{MVK-OO}+\text{HPMF})$ when the concentration of HPMF is the same as that of HCOOH.
 630 $k_{\text{eff}}(\text{MVK-OO}+\text{H}_2\text{O})$ and $k_{\text{eff}}(\text{MVK-OO}+\text{HCOOH})$ are greater than $k_{\text{eff}}(\text{MVK-OO}+\text{SO}_2)$, which, in turn,
 631 are greater than $k_{\text{eff}}(\text{MVK-OO}+\text{HPMF})$ when the concentration of HPMF is equal to that of
 632 SCIs. Based on the above discussions, it can be concluded that the relative importance
 633 of carbonyl oxides reactions with hydroperoxide esters is significantly dependent on
 634 the concentrations of hydroperoxide esters. These reactions may play a certain role in
 635 the formation of organic new particle in some regions where low concentration of water
 636 vapour and high concentration of hydroperoxide esters occur.



637
 638 **Figure 6.** PES (ΔG and ΔE , in italics) for the distinct SCIs + Pent1a reactions at the M06-2X/ma-
 639 TZVP//M06-2X/6-311+G(2df,2p) level of theory

640

641 **Table 2** The reported concentrations of coreactant, the rate coefficients k , and the effective pseudo-
 642 first-order rate constants ($k_{\text{eff}} = k[\text{coreactant}]$) for distinct SCI reactions with HPMF, H₂O, HCOOH
 643 and SO₂ at the tropical forest environments

SCIs	Coreactant	[Coreactant] (molecules cm ⁻³)	k (cm ³ molecule ⁻¹ s ⁻¹)	k_{eff} (s ⁻¹)	Reference
CH ₂ OO	H ₂ O	3.9-6.1 × 10 ¹⁷	< 1.5 × 10 ⁻¹⁵	5.9-9.2 × 10 ²	Chao et al., (2015)
	HCOOH	5.0-10.0 × 10 ¹⁰	[1.1 ± 0.1] × 10 ⁻¹⁰	5.5-11	Welz et al., (2014)]
	SO ₂	1.7-9.0 × 10 ¹⁰	[3.9 ± 0.7] × 10 ⁻¹¹	0.7-3.5	Welz et al., (2012)
<i>anti</i> -CH ₃ CHOO	HPMF	-	2.7 × 10 ⁻¹¹	-	This work
	H ₂ O	3.9-6.1 × 10 ¹⁷	[1.0 ± 0.4] × 10 ⁻¹⁴	3.9-6.1 × 10 ³	Taatjes et al., (2013)
	HCOOH	5.0-10.0 × 10 ¹⁰	[5 ± 3] × 10 ⁻¹⁰	25.0-50.0	Welz et al., (2014)
	SO ₂	1.7-9.0 × 10 ¹⁰	[6.7 ± 1.0] × 10 ⁻¹¹	1.1-6.0	Taatjes et al., (2013)
<i>syn</i> -CH ₃ CHOO	HPMF	-	3.3 × 10 ⁻¹⁰	-	This work
	H ₂ O	3.9-6.1 × 10 ¹⁷	< 4.0 × 10 ⁻¹⁵	1.6-2.4 × 10 ³	Taatjes et al., (2013)
	HCOOH	5.0-10.0 × 10 ¹⁰	[2.5 ± 0.3] × 10 ⁻¹⁰	12.5-25.0	Welz et al., (2014)
(CH ₃) ₂ COO	SO ₂	1.7-9.0 × 10 ¹⁰	[2.4 ± 0.3] × 10 ⁻¹¹	0.4-2.2	Taatjes et al., (2013)
	HPMF	-	1.7 × 10 ⁻¹³	-	This work
	H ₂ O	3.9-6.1 × 10 ¹⁷	< 1.5 × 10 ⁻¹⁶	58.5-91.5	Huang et al., (2015)
<i>syn-trans</i> -MVK-OO	HCOOH	5.0-10.0 × 10 ¹⁰	4.5 × 10 ⁻¹⁰	22.5-45.0	Sipilä et al., (2014)
	SO ₂	1.7-9.0 × 10 ¹⁰	1.3 × 10 ⁻¹⁰	2.2-11.7	Huang et al., (2015)
	HPMF	-	2.2 × 10 ⁻¹¹	-	This work
<i>syn-trans</i> -MVK-OO	H ₂ O	3.9-6.1 × 10 ¹⁷	< 4.0 × 10 ⁻¹⁷	15.6-24.4	Caravan et al., (2020)
	HCOOH	5.0-10.0 × 10 ¹⁰	[3.0 ± 0.1] × 10 ⁻¹⁰	15.0-30.0	Caravan et al., (2020)
	SO ₂	1.7-9.0 × 10 ¹⁰	[4.2 ± 0.6] × 10 ⁻¹¹	0.7-3.8	Caravan et al., (2020)

644 3.4 Vapour pressure and volatility of adduct products

645 The assessment of Barley and McFiggans (2010) and O'Meara et al. (2014) found
646 that the combination of boiling point estimation from Nannoolal et al. (2004) and
647 vapour pressure estimation from Nannoolal et al. (2008) gives the lowest mean bias
648 error of vapour pressure for atmospherically relevant compounds. Therefore, the
649 saturated vapour pressure (P^0) of adduct products at room temperature is estimated by
650 using the Nannoolal-Nannoolal method, and the results are listed in Table S10. From
651 Table S10, it can be seen that the P^0 of adduct products involved in the successive
652 reactions of CH_2OO with HCOOH increases first and then decreases with increasing
653 the number of CH_2OO . The P^0 of the adduct product $\text{HC}(\text{O})\text{O}(\text{CH}_2\text{OO})_3\text{H}$ is maximum
654 when the number of CH_2OO is equal to three. The P^0 of adduct products included in the
655 successive reactions of *anti*- CH_3CHOO with HCOOH decreases significantly as the
656 number of *anti*- CH_3CHOO is increased. Similar phenomenon is also observed from the
657 successive reactions of *syn*- CH_3CHOO and $(\text{CH}_3)_2\text{COO}$ with HCOOH . Notably, the P^0
658 of adduct products decreases obviously when the size of SCIs increases. For example,
659 the P^0 of the adduct product $\text{HC}(\text{O})\text{O}(\text{CH}_2\text{OO})_3\text{H}$ in the $n\text{CH}_2\text{OO} + \text{HCOOH}$ reaction
660 is estimated to be 4.43×10^{-3} atm, which is greater than those of the corresponding
661 adduct products in the *nanti*- $\text{CH}_3\text{CHOO} + \text{HCOOH}$ (7.12×10^{-4}), *nsyn*- $\text{CH}_3\text{CHOO} +$
662 HCOOH (7.12×10^{-4}), and $n(\text{CH}_3)_2\text{COO} + \text{HCOOH}$ (1.27×10^{-4}) reactions by 6.22,
663 6.22 and 34.88 times, respectively.

664 A classify scheme of various organic compounds is based on their volatility, as
665 presented by Donahue et al. (2012) The volatility of organic compounds is described
666 by their effective saturation concentration. The saturated concentrations (c^0) of adduct
667 products formed from the successive reactions of SCIs with HCOOH are predicted by
668 using the SIMPOL.1 method proposed by Pankow and Asher (2008), and the results
669 are listed in Table S10. As shown in Table S10, the c^0 of adduct products involved in
670 the $n\text{CH}_2\text{OO} + \text{HCOOH}$ reaction decreases with increasing the number of CH_2OO .
671 According to the Volatility Basis Set (VBS) of organic compounds (Donahue et al.,

672 2012), these adduct products belong to VOC ($c^0 > 3 \times 10^6 \text{ ug/m}^3$). Similarly, the c^0 of
673 adduct products included in the *nanti*-CH₃CHOO + HCOOH, *nsyn*-CH₃CHOO +
674 HCOOH, and *n*(CH₃)₂COO + HCOOH reactions decreases when the number of SCIs
675 increases. It deserves mentioning that the adduct products in the *nanti*-CH₃CHOO +
676 HCOOH and *nsyn*-CH₃CHOO + HCOOH reactions belong to intermediate volatility
677 organic compounds (IVOC, $300 < c^0 < 3 \times 10^6 \text{ ug/m}^3$) when the number of SCIs is equal
678 to five. However, the adduct products in the *n*(CH₃)₂COO + HCOOH reaction become
679 IVOC when the number of (CH₃)₂COO is greater than or equal to two. Based on the
680 above discussions, it can be concluded that the volatility of adduct products is
681 significantly affected by the number and size of SCIs in the successive reaction of SCIs
682 with HCOOH.

683 4. Conclusions

684 The oligomerization reaction mechanism and kinetics of Criegee intermediates
685 reactions with their respective hydroperoxide esters as well as HPMF are investigated
686 using quantum chemical calculations and kinetics modeling methods. The main
687 conclusion is summarized as follows.

688 (a) For the initiation reactions of distinct SCIs with HCOOH, the barrierless 1,4
689 O-H insertion reaction leading to the formation of hydroperoxide esters is the most
690 favorable pathway. The exothermicity of distinct SCIs reactions with HCOOH
691 decreases when the number of methyl groups increases, and the exothermicity of the
692 *anti*-CH₃CHOO + HCOOH reaction is higher than that of the *syn*-CH₃CHOO +
693 HCOOH system.

694 (b) The addition reactions of SCIs with hydroperoxide esters proceed through
695 successive insertion of SCIs into hydroperoxide ester to form oligomers that involve
696 SCIs as the repeating unit. These oligomerization reactions are strongly exothermic and
697 spontaneous. The exothermicity of oligomerization reactions significantly decreases
698 when the number of methyl substituents increases, and the exothermicity of *anti*-methyl
699 substituted carbonyl oxides is obviously higher than that of *syn*-methyl substituted
700 carbonyl oxides.

701 (c) The –OOH insertion reaction is favored over the –CH insertion pathway in the
702 SCIs oligomerization reactions, and the barrier heights increase with increasing the
703 number of SCIs added to the oligomer except *syn*-CH₃CHOO. The barrier of –OOH
704 insertion pathway shows a dramatic decrease when a methyl substituent occurs at the
705 *anti*-position, while it reveals a significant increase when a methyl group is introduced
706 at the *syn*-position and dimethyl substituent.

707 (d) Compared with the barrier of CH₂OO reaction with HPMF (8.1 kcal·mol⁻¹),
708 the barrier decreases by 2.5 kcal·mol⁻¹ when a methyl substituent occurs at the *anti*-
709 position, while the barrier increases by about 3.0 kcal·mol⁻¹ when a methyl group is
710 introduced at the *syn*-position and dimethyl substituent. The rate coefficients increase
711 by about one order of magnitude when a methyl substituent occurs at the *anti*-position,
712 whereas the rate coefficients decrease by 1 to 2 orders of magnitude when a methyl
713 group is introduced at the *syn*-position compared to the rate coefficients of the CH₂OO
714 + HPMF reaction.

715

716 **Data availability**

717 The data are accessible by contacting the corresponding author
718 (huangyu@ieecas.cn).

719

720 **Supplement**

721 The following information is provided in the Supplement: The electronic energy
722 (ΔE^\ddagger) and Gibbs free energy (ΔG^\ddagger) barriers for the initiation reactions of distinct SCIs
723 with HCOOH predicted at different levels; Enthalpies of formation for the various
724 carbonyl oxides and hydroperoxide esters; Rate coefficients of initiation reactions of
725 distinct SCIs with HCOOH; Rate coefficients of distinct SCIs reactions with HPMF;
726 Predicted saturated vapour pressure (P^0) and saturated concentrations (c^0) for the adduct
727 products; Relaxed scan energy profiles for varying the C-O and O-H bonds in the 1,4-
728 insertion reactions of distinct SCIs with HCOOH; Natural bond orbital (NBO) analysis

729 of the donor-acceptor orbitals; The NPA charges of different atoms in the distinct SCIs;
730 Optimized geometries of all the stationary points;

731

732 **Author contribution**

733 LC designed the study. LC and YH wrote the paper. LC performed theoretical
734 calculation. YX, ZJ, and WW analyzed the data. All authors reviewed and commented
735 on the paper.

736

737 **Competing interests**

738 The authors declare that they have no conflict of interest.

739

740 **Acknowledgments**

741 This work was supported by the National Natural Science Foundation of China
742 (grant Nos. 42175134, 41805107, and 22002080). It was also partially supported as
743 Strategic Priority Research Program of the Chinese Academy of Sciences, China (grant
744 Nos. XDA23010300 and XDA23010000), and CAS "Light of West China" Program
745 (XAB2019B01).

746

747

748 References

- 749 Alecu, I. M., Zheng, J., Zhao, Y., and Truhlar, D. G.: Computational thermochemistry: scale factor
750 databases and scale factors for vibrational frequencies obtained from electronic model
751 chemistries, *J. Chem. Theory Comput.*, 6, 2872-2887, <https://doi.org/10.1021/ct100326h>, 2010.
- 752 Anglada, J. M., and Solé, A.: Impact of the water dimer on the atmospheric reactivity of carbonyl
753 oxides, *Phys. Chem. Chem. Phys.*, 18, 17698-17712, <https://doi.org/10.1039/C6CP02531E>,
754 2016.
- 755 Aplincourt, P., and Ruiz-López, M. F.: Theoretical study of formic acid anhydride formation from
756 carbonyl oxide in the atmosphere, *J. Phys. Chem. A*, 104, 380-388,
757 <https://doi.org/10.1021/jp9928208>, 2000.
- 758 Atkinson, R., and Arey, J.: Atmospheric degradation of volatile organic compounds, *Chem. Rev.*,
759 103, 4605-4638, <https://doi.org/10.1021/cr0206420>, 2003.
- 760 Barber, V. P., Pandit, S., Green, A. M., Trongsirivat, N., Walsh, P. J., Klippenstein, S. J., and Lester,
761 M. I.: Four-carbon Criegee intermediate from isoprene ozonolysis: methyl vinyl ketone oxide
762 synthesis, infrared spectrum, and OH production, *J. Am. Chem. Soc.*, 140, 10866-10880,
763 <https://doi.org/10.1021/jacs.8b06010>, 2018.
- 764 Barley, M. H., and McFiggans, G.: The critical assessment of vapour pressure estimation methods
765 for use in modelling the formation of atmospheric organic aerosol, *Atmos. Chem. Phys.*, 10,
766 749-767, <https://doi.org/10.5194/acp-10-749-2010>, 2010.
- 767 Boys, S. F., and Bernardi, F.: The calculation of small molecular interactions by the differences of
768 separate total energies. Some procedures with reduced errors, *Mol. Phys.*, 19, 553-566,
769 <https://doi.org/10.1080/00268977000101561>, 1970.
- 770 Cabezas, C., and Endo, Y.: Observation of hydroperoxyethyl formate from the reaction between the
771 methyl Criegee intermediate and formic acid, *Phys. Chem. Chem. Phys.*, 22, 446-454,
772 <https://doi.org/10.1039/C9CP05030B>, 2020.
- 773 Cabezas, C., and Endo, Y.: The Criegee intermediate-formic acid reaction explored by rotational
774 spectroscopy, *Phys. Chem. Chem. Phys.*, 21, 18059-18064,
775 <https://doi.org/10.1039/c9cp03001h>, 2019.
- 776 Cabezas, C., and Endo, Y.: The reactivity of the Criegee intermediate CH_3CHOO with water probed
777 by FTMW spectroscopy, *J. Chem. Phys.*, 148, 014308-014315,
778 <https://doi.org/10.1063/1.5009033>, 2018.
- 779 Canneaux, S., Bohr, F., and Henon, E.: KiSThElP: a program to predict thermodynamic properties
780 and rate constants from quantum chemistry results, *J. Comput. Chem.*, 35, 82-93,
781 <https://doi.org/10.1002/jcc.23470>, 2013.
- 782 Caravan, R. L., Vansco, M. F., Au, K., Khan, M. A. H., Li, Y. L., Winiberg, F. A. F., Zuraski, K., Lin,
783 Y. H., Chao, W., Trongsirivat, N., Walsh, P. J., Osborn, D. L., Percival, C. J., Lin, J. J. M.,
784 Shallcross, D. E., Sheps, L., Klippenstein, S. J., Taatjes, C. A., and Lester, M. I.: Direct kinetic
785 measurements and theoretical predictions of an isoprene-derived Criegee intermediate, *Proc.*
786 *Natl. Acad. Sci. U.S.A.*, 117, 9733-9740, <https://doi.org/10.1073/pnas.1916711117>, 2020.
- 787 Chaliyakunnel, S., Millet, D. B., Wells, K. C., Cady-Pereira, K. E., and Shephard, M. W.: A large
788 underestimate of formic acid from tropical fires: constraints from space-borne measurements,
789 *Environ. Sci. Technol.*, 50, 5631-5640, <https://doi.org/10.1021/acs.est.5b06385>, 2016.

790 Chao, W., Hsieh, J. T., Chang, C. H., and Lin, J. J. M.: Direct kinetic measurement of the reaction
791 of the simplest Criegee intermediate with water vapor, *Science*, 347, 751-754,
792 <https://doi.org/10.1126/science.1261549>, 2015.

793 Chen, L., Huang, Y., Xue, Y., Cao J., and Wang, W.: Effect of oligomerization reactions of Criegee
794 intermediate with organic acid/peroxy radical on secondary organic aerosol formation from
795 isoprene ozonolysis, *Atmos. Environ.*, 187, 218-229,
796 <https://doi.org/10.1016/j.atmosenv.2018.06.001>, 2018.

797 Chen, L., Huang, Y., Xue, Y., Cao, J., and Wang, W.: Competition between HO₂ and H₂O₂ reactions
798 with CH₂OO/*anti*-CH₃CHOO in the oligomer formation: a theoretical perspective, *J. Phys.*
799 *Chem. A*, 121, 6981-6991, <https://doi.org/10.1021/acs.jpca.7b05951>, 2017.

800 Chen, L., Huang, Y., Xue, Y., Shen, Z., Cao, J., and Wang, W.: Mechanistic and kinetics
801 investigations of oligomer formation from Criegee intermediate reactions with hydroxyalkyl
802 hydroperoxides, *Atmos. Chem. Phys.*, 19, 4075-4091, [https://doi.org/10.5194/acp-19-4075-](https://doi.org/10.5194/acp-19-4075-2019)
803 2019, 2019.

804 Chen, L., Wang, W., Wang, W., Liu, Y., Liu, F., Liu, N., and Wang, B: Water-catalyzed
805 decomposition of the simplest Criegee intermediate CH₂OO, *Theor. Chem. Acc.*, 135, 131-143,
806 <https://doi.org/10.1007/s00214-016-1894-9>, 2016.

807 Chhantyal-Pun, R., McGillen, M. R., Beames, J. M., Khan, M. A. H., Percival, C. J., Shallcross, D.
808 E., and Orr-Ewing, A. J.: Temperature Dependence of the Rates of Reaction of Trifluoroacetic
809 Acid with Criegee Intermediates, *Angew. Chem. Int. Ed.*, 129, 9172-9175,
810 <https://doi.org/10.1002/anie.201703700>, 2017.

811 Chhantyal-Pun, R., Rotavera, B., McGillen, M. R., Khan, M. A. H., Eskola, A. J., Caravan, R. L.,
812 Blacker, L., Tew, D. P., Osborn, D. L., Percival, C. J., Taatjes, C. A., Shallcross D. E., and Orr-
813 Ewing, A. J.: Criegee intermediate reactions with carboxylic acids: a potential source of
814 secondary organic aerosol in the atmosphere, *ACS Earth Space Chem.*, 2, 833-842,
815 <https://doi.org/10.1021/acsearthspacechem.8b00069>, 2018.

816 Chung, C. A., Su, J. W., and Lee, Y. P.: Detailed mechanism and kinetics of the reaction of Criegee
817 intermediate CH₂OO with HCOOH investigated via infrared identification of conformers of
818 hydroperoxymethyl formate and formic acid anhydride, *Phys. Chem. Chem. Phys.*, 21, 21445-
819 21455, <https://doi.org/10.1039/c9cp04168k>, 2019.

820 Criegee, R.: Mechanism of ozonolysis, *Angew. Chem. Int. Ed. Engl.*, 14, 745-752,
821 <https://doi.org/10.1002/anie.197507451>, 1975.

822 Donahue, N. M., Kroll, J. H., Pandis, S. N., and Robinson, A. L.: A two-dimensional volatility basis
823 set – Part 2: Diagnostics of organic-aerosol evolution, *Atmos. Chem. Phys.*, 12, 615-634,
824 <https://doi.org/10.5194/acp-12-615-2012>, 2012.

825 Drozd, G. T., Kurtén, T., Donahue, N. M., and Lester, M. I.: Unimolecular decay of the dimethyl-
826 substituted Criegee intermediate in alkene ozonolysis: decay time scales and the importance of
827 tunneling, *J. Phys. Chem. A*, 121, 6036-6045, <https://doi.org/10.1021/acs.jpca.7b05495>, 2017.

828 Eckart, C.: The penetration of a potential barrier by electrons, *Phys. Rev.*, 35, 1303-1309,
829 <https://doi.org/10.1103/PhysRev.35.1303>, 1930.

830 Frisch, M. J., Trucks, G. W., Schlegel, H. B., Scuseria, G. E., Robb, M. A., Cheeseman, J. R.,
831 Montgomery, J. A. Jr., Vreven, T., Kudin, K. N., Burant, J. C., Millam, J. M., Iyengar, S. S.,
832 Tomasi, J., Barone, V., Mennucci, B., Cossi, M., Scalmani, G., Rega, N., Petersson, G. A.,
833 Nakatsuji, H., Hada, M., Ehara, M., Toyota, K., Fukuda, R., Hasegawa, J., Ishida, M., Nakajima,

834 T., Honda, Y., Kitao, O., Nakai, H., Klene, M., Li, X., Knox, J. E., Hratchian, H. P., Cross, J.
835 B., Adamo, C., Jaramillo, J., Gomperts, R., Stratmann, R. E., Yazyev, O., Austin, A. J., Cammi,
836 R., Pomelli, C., Ochterski, J. W., Ayala, P. Y., Morokuma, K., Voth, G. A., Salvador, P.,
837 Dannenberg, J. J., Zakrzewski, V. G., Dapprich, S., Daniels, A. D., Strain, M. C., Farkas, O.,
838 Malick, D. K., Rabuck, A. D., Raghavachari, K., Foresman, J. B., Ortiz, J. V., Cui, Q., Baboul,
839 A. G., Clifford, S., Cioslowski, J., Stefanov, B. B., Liu, G., Liashenko, A., Piskorz, P.,
840 Komaromi, I., Martin, R. L., Fox, D. J., Keith, T., Al-Laham, M. A., Peng, C. Y., Nanayakkara,
841 A., Challacombe, M., Gill, P. M. W., Johnson, B., Chen, W., Wong, M. W., Gonzalez, C., and
842 Pople, J. A.: Gaussian 09, Revision D.01; Gaussian, Inc.: Wallingford, CT, 2009.

843 Fukui, K.: The path of chemical reactions - the IRC approach, *Acc. Chem. Res.*, 14, 363-368,
844 <https://doi.org/10.1021/ar00072a001>, 1981.

845 Gilbert, R. G., and Smith, S. C.: *Theory of unimolecular and recombination reactions*; Blackwell
846 Scientific: Carlton, Australia, 1990.

847 Giorio, C., Campbell, S. J., Bruschi, M., Tampieri, F., Barbon, A., Toffoletti, A., Tapparo, A., Paijens,
848 C., Wedlake, A. J., Grice, P., Howe, D. J., and Kalbere, M.: Online quantification of Criegee
849 intermediates of α -pinene ozonolysis by stabilization with spin traps and proton-transfer
850 reaction mass spectrometry detection, *J. Am. Chem. Soc.*, 139, 3999-4008,
851 <https://doi.org/10.1021/jacs.6b10981>, 2017.

852 Glowacki, D. R., Liang, C. H., Morley, C., Pilling, M. J., and Robertson, S. H.: MESMER: an open-
853 source master equation solver for multi-energy well reactions, *J. Phys. Chem. A*, 116, 9545-
854 9560, <https://doi.org/10.1021/jp3051033>, 2012.

855 Gong, Y., and Chen, Z.: Quantification of the role of stabilized Criegee intermediates in the
856 formation of aerosols in limonene ozonolysis, *Atmos. Chem. Phys.*, 21, 813-829,
857 <https://doi.org/10.5194/acp-21-813-2021>, 2021.

858 Hammond, G. S.: A correlation of reaction rates, *J. Am. Chem. Soc.*, 77, 334-338,
859 <https://doi.org/10.1021/ja01607a027>, 1955.

860 Huang, H. L., Chao, W., and Lin, J. J. M.: Kinetics of a Criegee intermediate that would survive
861 high humidity and may oxidize atmospheric SO₂, *Proc. Natl. Acad. Sci. U.S.A.*, 112, 10857-
862 10862, <https://doi.org/10.1073/pnas.1513149112>, 2015.

863 Johnson, D., and Marston, G.: The gas-phase ozonolysis of unsaturated volatile organic compounds
864 in the troposphere, *Chem. Soc. Rev.*, 37, 699-716, <https://doi.org/10.1039/B704260B>, 2008.

865 Johnson, D., Lewin, A. G., and Marston, G.: The effect of Criegee-intermediate scavengers on the
866 OH yield from the reaction of ozone with 2-methylbut-2-ene, *J. Phys. Chem. A*, 105, 2933-
867 2935, <https://doi.org/10.1021/jp003975e>, 2001.

868 Karton, A., Kettner, M., and Wild, D. A.: Sneaking up on the Criegee intermediate from below:
869 Predicted photoelectron spectrum of the CH₂OO⁻ anion and W3-F12 electron affinity of
870 CH₂OO, *Chem. Phys. Lett.*, 585, 15-20, <http://doi.org/10.1016/j.cplett.2013.08.075>, 2013.

871 Khan, M. A. H., Percival, C. J., Caravan, R. L., Taatjes, C. A., and Shallcross, D. E.: Criegee
872 intermediates and their impacts on the troposphere, *Environ. Sci.: Processes Impacts*, 20, 437-
873 453, <https://doi.org/10.1039/C7EM00585G>, 2018.

874 Lester, M. I., and Klippenstein, S. J.: Unimolecular decay of Criegee intermediates to OH radical
875 products: prompt and thermal decay processes, *Acc. Chem. Res.*, 51, 978-985,
876 <https://doi.org/10.1021/acs.accounts.8b00077>, 2018.

877 Lin, J. J. M., and Chao, W.: Structure-dependent reactivity of Criegee intermediates studied with

878 spectroscopic methods, *Chem. Soc. Rev.*, 46, 7483-7497, <https://doi.org/10.1039/c7cs00336f>,
879 2017.

880 Lin, X., Meng, Q., Feng, B., Zhai, Y., Li, Y., Yu, Y., Li, Z., Shan, X., Liu, F., Zhang, L., and Sheng,
881 L.: Theoretical study on Criegee intermediate's role in ozonolysis of acrylic acid, *J. Phys. Chem.*
882 *A*, 123, 1929-1936, <https://doi.org/10.1021/acs.jpca.8b11671>, 2019.

883 Liu, F., Beames, J. M., Petit, A. S., McCoy, A. B., and Lester, M. I.: Infrared-driven unimolecular
884 reaction of CH₃CHOO Criegee intermediates to OH radical products, *Science*, 345, 1596-1598,
885 <https://doi.org/10.1126/science.1257158>, 2014.

886 Liu, L., Bei, N., Wu, J., Liu, S., Zhou, J., Li, X., Yang, Q., Feng, T., Cao, J., Tie, X., and Li, G.:
887 Effects of stabilized Criegee intermediates (sCIs) on sulfate formation: a sensitivity analysis
888 during summertime in Beijing-Tianjin-Hebei (BTH), China, *Atmos. Chem. Phys.*, 19, 13341-
889 13354, <https://doi.org/10.5194/acp-19-13341-2019>, 2019.

890 Long, B., Bao, J. L., and Truhlar, D. G.: Atmospheric chemistry of Criegee intermediates:
891 unimolecular reactions and reactions with water, *J. Am. Chem. Soc.*, 138, 14409-14422,
892 <https://doi.org/10.1021/jacs.6b08655>, 2016.

893 Long, B., Bao, J. L., and Truhlar, D. G.: Unimolecular reaction of acetone oxide and its reaction
894 with water in the atmosphere, *Proc. Natl. Acad. Sci. U.S.A.*, 115, 6135-6140,
895 <https://doi.org/10.1073/pnas.1804453115>, 2018.

896 Long, B., Cheng, J. R., Tan, X. F., and Zhang, W. J.: Theoretical study on the detailed reaction
897 mechanisms of carbonyl oxide with formic acid, *J. Mol. Struct.: Theochem*, 916, 159-167,
898 <https://doi.org/10.1016/j.theochem.2009.09.028>, 2009.

899 Lu, T., and Chen, F.: Multiwfn: A multifunctional wavefunction analyzer, *J. Comput. Chem.*, 33,
900 580-592, <https://doi.org/10.1002/jcc.22885>, 2012.

901 Mendes, J., Zhou, C. W., and Curran, H. J.: Theoretical chemical kinetic study of the H-atom
902 abstraction reactions from aldehydes and acids by H atoms and OH, HO₂, and CH₃ radicals, *J.*
903 *Phys. Chem. A*, 118, 12089-12104, <https://doi.org/10.1021/jp5072814>, 2014.

904 Nannoolal, Y., Rarey, J., and Ramjugernatha, D.: Estimation of pure component properties Part 3.
905 Estimation of the vapor pressure of non-electrolyte organic compounds via group contributions
906 and group interactions, *Fluid Phase Equilibria*, 269, 117-133,
907 <https://doi.org/10.1016/j.fluid.2008.04.020>, 2008.

908 Nannoolal, Y., Rarey, J., Ramjugernatha, D., and Cordesb, W.: Estimation of pure component
909 properties Part 1. Estimation of the normal boiling point of non-electrolyte organic compounds
910 via group contributions and group interactions, *Fluid Phase Equilibria*, 226, 45-63,
911 <https://doi.org/10.1016/j.fluid.2004.09.001>, 2004.

912 Neeb, P., Horie, O., and Moortgat, G. K.: The ethene-ozone reaction in the gas phase, *J. Phys. Chem.*
913 *A*, 102, 6778-6785, <https://doi.org/10.1021/jp981264z>, 1998.

914 Novelli, A., Hens, K., Ernest, C. T., Martinez, M., Nölscher, A. C., Sinha, V., Paasonen, P., Petäjä,
915 T., Sipilä, M., Elste, T., Plass-Dülmer, C., Phillips, G. J., Kubistin, D., Williams, J., Vereecken,
916 L., Lelieveld, J., and Harder, H.: Estimating the atmospheric concentration of Criegee
917 intermediates and their possible interference in a FAGE-LIF instrument, *Atmos. Chem. Phys.*,
918 17, 7807-7826, <https://doi.org/10.5194/acp-17-7807-2017>, 2017.

919 Novelli, A., Vereecken, L., Lelieveld, J., and Harder, H.: Direct observation of OH formation from
920 stabilised Criegee intermediates, *Phys. Chem. Chem. Phys.*, 16, 19941-19951,
921 <https://doi.org/10.1039/c4cp02719a>, 2014.

922 O'Meara, S., Booth, A. M., Barley, M. H., Topping, D., and McFiggans, G.: An assessment of vapour
923 pressure estimation methods, *Phys. Chem. Chem. Phys.*, 16, 19453-19469,
924 <https://doi.org/10.1039/C4CP00857J>, 2014.

925 Osborn, D. L., and Taatjes, C. A.: The physical chemistry of Criegee intermediates in the gas phase,
926 *Int. Rev. Phys. Chem.*, 34, 309-360, <https://doi.org/10.1080/0144235X.2015.1055676>, 2015.

927 Pankow, J. F., and Asher, W. E.: SIMPOL.1: a simple group contribution method for predicting
928 vapor pressures and enthalpies of vaporization of multifunctional organic compounds, *Atmos.*
929 *Chem. Phys.*, 8, 2773-2796, <https://doi.org/10.5194/acp-8-2773-2008>, 2008.

930 Paulot, F., Wunch, D., Crounse, J. D., Toon, G. C., Millet, D. B., DeCarlo, P. F., Vigouroux, C.,
931 Deutscher, N. M., Abad, G. G., Notholt, J., Warneke, T., Hannigan, J. W., Warneke, C., de
932 Gouw, J. A., Dunlea, E. J., Mazière, M. D., Griffith, D. W. T., Bernath, P., Jimenez, J. L., and
933 Wennberg, P. O.: Importance of secondary sources in the atmospheric budgets of formic and
934 acetic acids, *Atmos. Chem. Phys.*, 11, 1989-2013, <https://doi.org/10.5194/acp-11-1989-2011>,
935 2011.

936 Peltola, J., Seal, P., Inkilä, A., and Eskola, A.: Time-resolved, broadband UV-absorption
937 spectrometry measurements of Criegee intermediate kinetics using a new photolytic precursor:
938 unimolecular decomposition of CH₂OO and its reaction with formic acid, *Phys. Chem. Chem.*
939 *Phys.*, 22, 11797-11808, <https://doi.org/10.1039/d0cp00302f>, 2020.

940 Porterfield, J. P., Lee, K. L. K., Dell'Isola, V., Carroll, P. B., and McCarthy, M. C.: Characterization
941 of the simplest hydroperoxide ester, hydroperoxymethyl formate, a precursor of atmospheric
942 aerosols, *Phys. Chem. Chem. Phys.*, 21, 18065-18070, <https://doi.org/10.1039/c9cp03466h>,
943 2019.

944 Riva, M., Budisulistiorini, S. H., Zhang, Z., Gold, A., Thornton, J. A., Turpin, B. J., and Surratt, J.
945 D.: Multiphase reactivity of gaseous hydroperoxide oligomers produced from isoprene
946 ozonolysis in the presence of acidified aerosols, *Atmos. Environ.*, 152, 314-322,
947 <https://doi.org/10.1016/j.atmosenv.2016.12.040>, 2017.

948 Sadezky, A., Winterhalter, R., Kanawati, B., Rompp, A., Spengler, B., Mellouki, A., Bras, G. L.,
949 Chaimbault, P., and Moortgat, G. K.: Oligomer formation during gas-phase ozonolysis of small
950 alkenes and enol ethers: new evidence for the central role of the Criegee Intermediate as
951 oligomer chain unit, *Atmos. Chem. Phys.*, 8, 2667-2699, <https://doi.org/10.5194/acp-8-2667-2008>, 2008.

952

953 Sakamoto, Y., Inomata, S., and Hirokawa, J.: Oligomerization reaction of the Criegee intermediate
954 leads to secondary organic aerosol formation in ethylene ozonolysis, *J. Phys. Chem. A*, 117,
955 12912-12921, <https://doi.org/10.1021/jp408672m>, 2013.

956 Sakamoto, Y., Yajima, R., Inomatad, S., and Hirokawa, J.: Water vapour effects on secondary
957 organic aerosol formation in isoprene ozonolysis, *Phys. Chem. Chem. Phys.*, 19, 3165-3175,
958 <https://doi.org/10.1039/c6cp04521a>, 2017.

959 Sipilä, M., Jokinen, T., Berndt, T., Richters, S., Makkonen, R., Donahue, N. M., Mauldin Iii, R. L.,
960 Kurtén, T., Paasonen, P., Sarnela, N., Ehn, M., Junninen, H., Rissanen, M. P., Thornton, J.,
961 Stratmann, F., Herrmann, H., Worsnop, D. R., Kulmala, M., Kerminen, V. M., and Petäjä, T.:
962 Reactivity of stabilized Criegee intermediates (sCIs) from isoprene and monoterpene
963 ozonolysis toward SO₂ and organic acids, *Atmos. Chem. Phys.*, 14, 12143-12153,
964 <https://doi.org/10.5194/acp-14-12143-2014>, 2014.

965 So, S., Wille, U., and Silva, G. D.: Atmospheric chemistry of enols: a theoretical study of the vinyl

966 alcohol + OH + O₂ reaction mechanism, *Environ. Sci. Technol.*, 48, 6694-6701,
967 <https://doi.org/10.1021/es500319q>, 2014.

968 Stavrakou, T., Müller, J. F., Peeters, J., Razavi, A., Clarisse, L., Clerbaux, C., Coheur, P. F., Hurtmans,
969 D., Mazière, M. D., Vigouroux, C., Deutscher, N. M., Griffith, D. W. T., Jones, N., and Paton-
970 Walsh, C.: Satellite evidence for a large source of formic acid from boreal and tropical forests,
971 *Nat. Geosci.*, 5, 26-30, <https://doi.org/10.1038/ngeo1354>, 2012.

972 Taatjes, C. A., Khan, M. A. H., Eskola, A. J., Percival, C. J., Osborn, D. L., Wallington, T. J., and
973 Shallcross, D. E.: Reaction of perfluorooctanoic acid with Criegee intermediates and
974 implications for the atmospheric fate of perfluorocarboxylic acids, *Environ. Sci. Technol.*, 53,
975 1245-1251, <https://doi.org/10.1021/acs.est.8b05073>, 2019.

976 Taatjes, C. A., Welz, O., Eskola, A. J., Savee, J. D., Scheer, A. M., Shallcross, D. E., Rotavera, B.,
977 Lee, E. P. F., Dyke, J. M., Mok, D. K. W., Osborn, D. L., and Percival, C. J.: Direct
978 measurements of conformer-dependent reactivity of the Criegee intermediate CH₃CHOO,
979 *Science*, 340, 177-180, <https://doi.org/10.1126/science.1234689>, 2013.

980 Taatjes, C. A.: Criegee intermediates: what direct production and detection can teach us about
981 reactions of carbonyl oxides, *Annu. Rev. Phys. Chem.*, 68, 183-207,
982 <https://doi.org/10.1146/annurev-physchem-052516-050739>, 2017.

983 Tobias, H. J., and Ziemann, P. J.: Kinetics of the gas-phase reactions of alcohols, aldehydes,
984 carboxylic acids, and water with the C13 stabilized Criegee intermediate formed from
985 ozonolysis of 1-tetradecene, *J. Phys. Chem. A*, 105, 6129-6135,
986 <https://doi.org/10.1021/jp004631r>, 2001.

987 Truhlar, D. G., Hase, W. L., and Hynes, J. T.: Current status of transition-state theory, *J. Phys. Chem.*,
988 87, 2664-2682, <https://doi.org/10.1021/jp953748q>, 1996.

989 Vansco, M. F., Zuraski, K., Winiberg, F. A. F., Au, K., Trongsiwat, N., Walsh, P. J., Osborn, D. L.,
990 Percival, C. J., Klippenstein, S. J., Taatjes, C. A., Lester, M. I., and Caravan, R. L.:
991 Functionalized hydroperoxide formation from the reaction of methacrolein-oxide, an isoprene-
992 derived Criegee intermediate, with formic acid: experiment and theory, *Molecules*, 26, 3058-
993 3072, <https://doi.org/10.3390/molecules26103058>, 2021.

994 Vereecken, L., Harder, H., and Novelli, A.: The reaction of Criegee intermediates with NO, RO₂,
995 and SO₂, and their fate in the atmosphere, *Phys. Chem. Chem. Phys.*, 14, 14682-14695,
996 <https://doi.org/10.1039/c2cp42300f>, 2012.

997 Vereecken, L.: The reaction of Criegee intermediates with acids and enols, *Phys. Chem. Chem.*
998 *Phys.*, 19, 28630-28640, <https://doi.org/10.1039/c7cp05132h>, 2017.

999 Wang, S., Newland, M. J., Deng, W., Rickard, A. R., Hamilton, J. F., Muñoz, A., Ródenas, M.,
1000 Vázquez, M. M., Wang, L., and Wang, X.: Aromatic photo-oxidation, a new source of
1001 atmospheric acidity, *Environ. Sci. Technol.*, 54, 7798-7806,
1002 <https://doi.org/10.1021/acs.est.0c00526>, 2020.

1003 Welz, O., Eskola, A. J., Sheps, L., Rotavera, B., Savee, J. D., Scheer, A. M., Osborn, D. L., Lowe,
1004 D., Booth, A. M., Xiao, P., Khan, M. A. H., Percival, C. J., Shallcross, D. E., and Taatjes, C.
1005 A.: Rate coefficients of C(1) and C(2) Criegee intermediate reactions with formic and acetic
1006 Acid near the collision limit: direct kinetics measurements and atmospheric implications,
1007 *Angew. Chem. Int. Ed.*, 53, 4547-4550, <https://doi.org/10.1002/anie.201400964>, 2014.

1008 Welz, O., Savee, J. D., Osborn, D. L., Vasu, S. S., Percival, C. J., Shallcross, D. E., and Taatjes, C.
1009 A.: Direct kinetic measurements of Criegee intermediate (CH₂OO) formed by reaction of CH₂I

1010 with O₂, *Science*, 335, 204-207, <https://doi.org/10.1126/science.1213229>, 2012.

1011 Yin, C., and Takahashi, K.: How does substitution affect the unimolecular reaction rates of Criegee
1012 intermediates? *Phys. Chem. Chem. Phys.*, 19, 12075-12084,
1013 <https://doi.org/10.1039/c7cp01091e>, 2017.

1014 Yu, S.: Role of organic acids (formic, acetic, pyruvic and oxalic) in the formation of cloud
1015 condensation nuclei (CCN): a review, *Atmos. Res.*, 53, 185-217,
1016 [https://doi.org/10.1016/S0169-8095\(00\)00037-5](https://doi.org/10.1016/S0169-8095(00)00037-5), 2000.

1017 Zhang, P., Wang, W., Zhang, T., Chen, L., Du, Y., Li, C., and Lv, J.: Theoretical study on the
1018 mechanism and kinetics for the self-reaction of C₂H₅O₂ radicals, *J. Phys. Chem. A*, 116, 4610-
1019 4620, <https://doi.org/10.1021/jp301308u>, 2012.

1020 Zhao, R., Kenseth, C. M., Huang, Y., Dalleska, N. F., Kuang, X. M., Chen, J., Paulson, S. E., and
1021 Seinfeld, J. H.: Rapid aqueous-phase hydrolysis of ester hydroperoxides arising from Criegee
1022 intermediates and organic acids, *J. Phys. Chem. A*, 122, 5190-5201,
1023 <https://doi.org/10.1021/acs.jpca.8b02195>, 2018.

1024 Zhao, Y., and Truhlar, D. G.: The M06 suite of density functionals for main group thermochemistry,
1025 thermochemical kinetics, noncovalent interactions, excited states, and transition elements: two
1026 new functionals and systematic testing of four M06-class functionals and 12 other functionals,
1027 *Theor. Chem. Acc.*, 120, 215-241, <https://doi.org/10.1007/s00214-007-0310-x>, 2008.

1028 Zhao, Y., Wingen, L. M., Perraud, V., Greaves, J., and Finlayson-Pitts, B. J.: Role of the reaction of
1029 stabilized Criegee intermediates with peroxy radicals in particle formation and growth in air,
1030 *Phys. Chem. Chem. Phys.*, 17, 12500-12514, <https://doi.org/10.1039/c5cp01171j>, 2015.

1031 Zhou, S., Joudan, S., Forbes, M. W., Zhou, Z., and Abbatt, J. P. D.: Reaction of condensed-phase
1032 Criegee intermediates with carboxylic acids and perfluoroalkyl carboxylic acids, *Environ. Sci.
1033 Technol. Lett.*, 6, 243-250, <https://doi.org/10.1021/acs.estlett.9b00165>, 2019.